University Library

MINERVA ACCESS

A gateway to Melbourne's research publications

Minerva Access is the Institutional Repository of The University of Melbourne

Author/s:
Salscheider, SL;Gerlich, S;Cabrera-Orefice, A;Peker, E;Rothemann, RA;Murschall, LM;Finger, Y;Szczepanowska, K;Ahmadi, ZA;Guerrero-Castillo, S;Erdogan, A;Becker, M;Ali, M;Habich, M;Petrungaro, C;Burdina, N;Schwarz, G;Klußmann, M;Neundorf, I;Stroud, DA;Ryan, MT;Trifunovic, A;Brandt, U;Riemer, J

Title:
AIFM1 is a component of the mitochondrial disulfide relay that drives complex I assembly through efficient import of NDUFS5

Date:
2022-09-01

Citation:
Salscheider, S. L., Gerlich, S., Cabrera-Orefice, A., Peker, E., Rothemann, R. A., Murschall, L. M., Finger, Y., Szczepanowska, K., Ahmadi, Z. A., Guerrero-Castillo, S., Erdogan, A., Becker, M., Ali, M., Habich, M., Petrungaro, C., Burdina, N., Schwarz, G., Klußmann, M., Neundorf, I. ,... Riemer, J. (2022). AIFM1 is a component of the mitochondrial disulfide relay that drives complex I assembly through efficient import of NDUFS5. EMBO Journal, 41 (17), https://doi.org/10.15252/embj.2022110784.

Persistent Link:
https://hdl.handle.net/11343/317103

License:
CC BY-NC-ND

Article

TRANSPARENT PROCESS OPEN ACCESS

THE EMBO JOURNAL

# AIFM1 is a component of the mitochondrial disulfide relay that drives complex I assembly through efficient import of NDUFS5

Silja Lucia Salscheider[1,†], Sarah Gerlich[1,†], Alfredo Cabrera-Orefice[2,†], Esra Peker[1], Robin Alexander Rothemann[1], Lena Maria Murschall[1], Yannik Finger[1], Karolina Szczepanowska[3,4], Zeinab Alsadat Ahmadi[2], Sergio Guerrero-Castillo[2], Alican Erdogan[1], Mark Becker[1], Muna Ali[1], Markus Habich[1], Carmelina Petrungaro[1], Nele Burdina[1], Guenter Schwarz[1,4,5], Merlin Klußmann[1], Ines Neundorf[1], David A Stroud[6,‡], Michael T Ryan[6], Aleksandra Trifunovic[3,4,5], Ulrich Brandt[2,4,*] & Jan Riemer[1,4,**]

## Abstract

**The mitochondrial intermembrane space protein AIFM1 has been reported to mediate the import of MIA40/CHCHD4, which forms the import receptor in the mitochondrial disulfide relay. Here, we demonstrate that AIFM1 and MIA40/CHCHD4 cooperate beyond this MIA40/CHCHD4 import. We show that AIFM1 and MIA40/CHCHD4 form a stable long-lived complex *in vitro*, in different cell lines, and in tissues. In HEK293 cells lacking AIFM1, levels of MIA40 are unchanged, but the protein is present in the monomeric form. Monomeric MIA40 neither efficiently interacts with nor mediates the import of specific substrates. The import defect is especially severe for NDUFS5, a subunit of complex I of the respiratory chain. As a consequence, NDUFS5 accumulates in the cytosol and undergoes rapid proteasomal degradation. Lack of mitochondrial NDUFS5 in turn results in stalling of complex I assembly. Collectively, we demonstrate that AIFM1 serves two overlapping functions: importing MIA40/CHCHD4 and constituting an integral part of the disulfide relay that ensures efficient interaction of MIA40/CHCHD4 with specific substrates.**

**Keywords** AIFM1; complex I; MIA40-CHCHD4; mitochondrial disulfide relay; NDUFS5

**Subject Category** Organelles

**DOI** 10.15252/embj.2022110784 | Received 27 January 2022 | Revised 26 June 2022 | Accepted 30 June 2022 | Published online 20 July 2022

**The EMBO Journal (2022) 41: e110784**

## Introduction

Apoptosis-inducing factor (AIFM1) was originally identified as a mitochondrial intermembrane space (IMS) protein capable of inducing caspase-independent chromatin condensation and DNA fragmentation when added to isolated nuclei (Susin *et al*, 1999). Various studies suggested that AIFM1 was required for complex I biogenesis, as loss resulted in decreased levels of assembled complex I (Vahsen *et al*, 2004; Troulinaki *et al*, 2018). More specifically, studies in mice using specific liver and muscle deletions of AIFM1 demonstrated a loss of complex I and OXPHOS deficiency (Pospisilik *et al*, 2007). In line, patients harboring AIFM1 mutations exhibit combined oxidative phosphorylation deficiency, deafness, and cowchock syndrome (McKenzie & Ryan, 2010; Bano & Prehn, 2018). However, through which molecular mechanism AIFM1 impacts on complex I biogenesis remained unclear.

Recent work using cell culture models and the harlequin mouse (an AIFM1 hypomorph containing only 20% of wildtype AIFM1 levels; Klein *et al*, 2002) led to the proposal that AIFM1 serves as an import receptor for the protein "mitochondrial intermembrane space import and assembly protein 40" (MIA40, also human CHCHD4) (Hangen *et al*, 2015; Meyer *et al*, 2015; Petrungaro *et al*, 2015). AIFM1-mediated import of MIA40/CHCHD4 relies on the unstructured N-terminal region in MIA40/CHCHD4 instead of a classic mitochondrial targeting sequence (MTS) (Hangen *et al*, 2015).

MIA40/CHCHD4 is an IMS oxidoreductase and an important part of the so-called mitochondrial disulfide relay. It serves as an import

1 Institute for Biochemistry, University of Cologne, Cologne, Germany
2 Radboud Institute for Molecular Life Sciences, Radboud University Medical Center, Nijmegen, The Netherlands
3 Medical Faculty, Institute for Mitochondrial Diseases and Aging, University of Cologne, Cologne, Germany
4 Cologne Excellence Cluster on Cellular Stress Responses in Aging-Associated Diseases (CECAD), University of Cologne, Cologne, Germany
5 Center for Molecular Medicine, University of Cologne, Cologne, Germany
6 Department of Biochemistry and Molecular Biology, Monash Biomedicine Discovery Institute, Monash University, Melbourne, Vic., Australia
*Corresponding author. Tel: +31–24–36-67098; E-mail: ulrich.brandt@radboudumc.nl
**Corresponding author (lead contact). Tel: +49–221–470-7306; E-mail: jan.riemer@uni-koeln.de
†These authors contributed equally to this work
‡Present address: Department of Biochemistry and Molecular Biology, Bio21 Molecular Science and Biotechnology Institute, University of Melbourne, Parkville, Vic., Australia

© 2022 The Authors. Published under the terms of the CC BY NC ND 4.0 license.

receptor for a number of IMS proteins and mediates their oxidative folding (Hofmann *et al*, 2005; Mesecke *et al*, 2005; Rissler *et al*, 2005; Banci *et al*, 2009, 2010; Fischer *et al*, 2013; Petrungaro *et al*, 2015; Habich *et al*, 2019). To this end, it uses a redox-active cysteine pair and a hydrophobic groove (Banci *et al*, 2010; Peleh *et al*, 2016; Erdogan *et al*, 2018; Habich *et al*, 2019) and cooperates with the sulfhydryl oxidase augmeter of liver regeneration (ALR) (Fischer *et al*, 2013; Bihlmaier *et al*, 2007). Among the MIA40/CHCHD4 substrates are four structural subunits of complex I (NDUFA8, NDUFB7, NDUFB10, and NDUFS5) (Szklarczyk *et al*, 2011; Petrungaro *et al*, 2015; Zhu *et al*, 2016; Friederich *et al*, 2017). It was proposed that complex I defects in AIFM1 deficient cells are caused by impaired MIA40/CHCHD4 import and its resulting proteasomal degradation. This is in line with the loss of complex I subunits that are critical for complex I assembly (Stroud *et al*, 2016) in MIA40/CHCHD4 knockdown cells (Fischer *et al*, 2013; Habich *et al*, 2019). The functional link between MIA40/CHCHD4 and AIFM1 is further supported by the fact that overexpression of MIA40/CHCHD4, either with or without an MTS, complements the loss of AIFM1 (Hangen *et al*, 2015; Meyer *et al*, 2015).

Interestingly, in harlequin mice, the reduction in MIA40/CHCHD4 levels appears to differ between tissues and age, resulting in hardly any MIA40/CHCHD4 loss despite decreased levels of AIFM1 under certain conditions (Meyer *et al*, 2015; Wischhof *et al*, 2018). This indicates that MIA40/CHCHD4 can also be imported in an AIFM1 independent fashion further emphasized by the fact that the import of human MIA40/CHCHD4 can take place in yeast cells, which do not contain AIFM1 (Chacinska *et al*, 2008). These findings imply functions of AIFM1 beyond MIA40/CHCHD4 import, which remain unclear.

Here, we demonstrate that the function of AIFM1 extends beyond its previously described role in facilitating MIA40/CHCHD4 import. AIFM1 serves as a platform stably binding almost all cellular MIA40/CHCHD4 in a long-lived stable complex in all cells and tissues investigated. We characterized an AIFM1 knockout HEK293 cell line that has unchanged MIA40/CHCHD4 levels and still displayed an isolated complex I deficiency. Using complexome profiling (Heide *et al*, 2012), we found that the loss of complex I subunits was secondary to stalling of complex I biogenesis at a specific assembly intermediate, which requires the MIA40/CHCHD4 substrate NDUFS5 to progress to fully assembled complex I. NDUFS5 relies on interaction with MIA40/CHCHD4 for import and oxidation. This interaction was absent in AIFM1 knockout cells due to the accumulation of monomeric soluble MIA40/CHCHD4 instead of the stable membrane-associated MIA40/CHCHD4-AIFM1 complex. Ultimately, nonimported NDUFS5 undergoes rapid proteasomal degradation. Collectively, we not only place AIFM1 as a critical component of the mammalian disulfide relay, but also provide insights into the cooperation of MIA40/CHCHD4 and AIFM1 in complex I biogenesis and demonstrate the close and specific surveillance of mitochondrial import by cytosolic quality control systems.

## Results

### In AIFM1 knockout HEK293 cells, levels of complex I are strongly reduced despite normal MIA40/CHCHD4 levels

Depletion of AIFM1 in cell culture by siRNA treatment or in the harlequin mouse model resulted in a loss of MIA40/CHCHD4 (Hangen *et al*, 2015; Meyer *et al*, 2015). Thus, it was proposed that AIFM1 loss-induced reduction in complex I levels is secondary to the loss of MIA40/CHCHD4. However, the loss of MIA40/CHCHD4 upon AIFM1 depletion appears to depend on additional parameters as it does not always occur. The presence of adaptation mechanisms ensuring MIA40/CHCHD4 import in the absence of AIFM1 (Murschall *et al*, 2020) was corroborated by almost unchanged MIA40/CHCHD4 levels, localization, and redox state in HEK293

**Figure 1. AIFM1 knockout results in decreased complex I levels despite normal amounts of MIA40/CHCHD4.**

A Assessment of protein levels in different AIFM1 knockout clones. Lysates from different AIFM1 knockout clones and wildtype cells were analyzed by reducing SDS–PAGE and immunoblotting. MIA40/CHCHD4 levels are not changed in AIFM1 knockout HEK293 cells.

B Proteomic analysis comparing MIA40/CHCHD4 levels in HEK293 and AIFM1 knockout mitochondria. Mitochondria from the SILAC-labeled cells were subjected to proteomic analyses (Dataset EV1). MIA40/CHCHD4 levels are unchanged in AIFM1 knockout cells compared with HEK293 cells. $N = 4$ biological replicates, an unpaired one-sample two-sided Student's *t*-test was applied ($P < 0.05$, fold change >2).

C Proteomic analysis comparing MIA40/CHCHD4 substrate levels in HEK293 and AIFM1 knockout mitochondria (same as B). Mitochondria from the SILAC-labeled cells were subjected to proteomic analyses (Dataset EV1). Levels of many MIA40/CHCHD4 substrates were significantly reduced in AIFM1 knockout cells compared with HEK293 cells. Notably, this appears to be selective as other MIA40/CHCHD4 substrates were not or only slightly affected by AIFM1 deletion. $N = 4$ biological replicates, an unpaired one-sample two-sided Student's *t*-test was applied ($P < 0.05$, fold change > 2).

D Assessment of protein levels in HEK293 cells, AIFM1 knockout cells, and AIFM1 knockout cells with reintroduced AIFM1-HA (expression of AIFM1-HA induced for 1 day). Different amounts of lysates from the indicated cells were analyzed by reducing SDS–PAGE and immunoblotting. While levels of MIA40 were largely unchanged, levels of many MIA40/CHCHD4 substrates were diminished in AIFM1 knockout cells. $N = 3$ biological replicates. Gray box indicates subunits of complex I.

E Proteomic analysis comparing respiratory chain protein levels in HEK293 and AIFM1 knockout mitochondria (same as B.). Mitochondria from the SILAC-labeled cells were subjected to proteomic analyses (Dataset EV1). Mainly levels of complex I subunits were significantly reduced in AIFM1 knockout cells compared with HEK293 cells. $N = 4$ biological replicates, an unpaired one-sample two-sided Student's *t*-test was applied ($P < 0.05$, fold change >2).

F BN–PAGE analyses of HEK293 cells, AIFM1 knockout cells, and AIFM1 knockout cells with reintroduced AIFM1-HA or AIFM1. Complex I was resolved from isolated mitochondria with blue native electrophoresis (BN–PAGE) followed by immunoblotting or in gel determination of the complex I specific activity. Levels of complex I were decreased in AIFM1 knockout cells. $N = 3$ biological replicates.

G Activity analyses of respiratory chain complex I in HEK293, AIFM1 knockout, and AIFM1 knockout complemented with AIFM1-HA or AIFM1. Activity of complex I was assessed in broken mitochondrial membranes and normalized to the activity of complex II. In AIFM1 knockout cells, complex I shows a significantly decreased activity to about 30–40% of wildtype cells, in line with a decrease in total complex I levels to about 30–40%. Thus, the specific activity of still assembled complex I in AIFM1 knockout cells is unchanged. Complementation of AIFM1 knockout cells with both, AIFM1 or AIFM1-HA rescues activity of complex I. $N = 7$ biological replicates; error bars indicate SD and an unpaired, two-sided Student's *t*-test was applied (**$P < 0.01$, ****$P < 0.0001$).


© 2022 The Authors

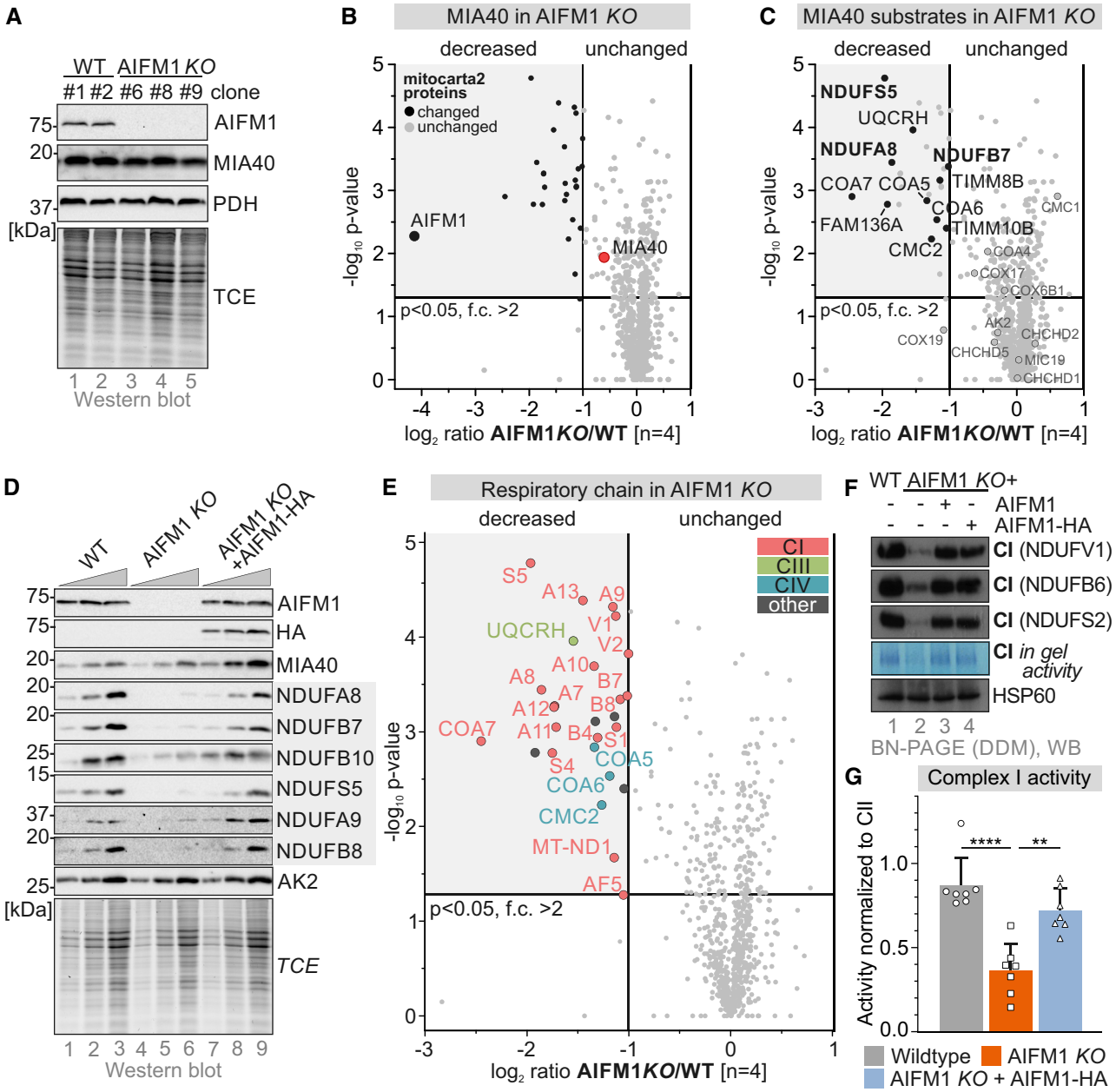



**Figure 1.**

cells in which we had generated a complete AIFM1 knockout using CRISPR-Cas9 technology (Fig 1A and B and Appendix Fig S1A–C). MIA40/CHCHD4 maturation kinetics were slightly delayed, which did, however, not translate into steady-state changes in MIA40/CHCHD4 levels (Appendix Fig S1B). Despite the presence of normal MIA40/CHCHD4 levels, amounts of selected (but not all) MIA40/CHCHD4 substrates were diminished (Fig 1C) including three of the four MIA40/CHCHD4-dependent subunits of complex I (NDUFA8, NDUFB7, NDUFS5). The fourth, NDUFB10, was not detected in this proteomic experiment. Immunoblot analysis confirmed the strongly reduced protein levels of all four MIA40/CHCHD4-dependent complex I subunits and complementation by introducing AIFM1-HA (Fig 1D). In addition, likely secondary to the loss of these MIA40/CHCHD4 substrates, further subunits of complex I were lost in AIFM1 knockout cells (Fig 1D and E; Appendix Fig S2A). This is in line with previous data showing that targeted knockout of the MIA40/CHCHD4 substrates NDUFA8, NDUFS5, NDUFB7, and NDUFB10 resulted in the overall loss of complex I (Stroud *et al*, 2016). Complex I loss was further confirmed by BN–PAGE and immunoblotting against different subunits (Fig 1F). Rotenone-sensitive complex I activity was lowered significantly in mitochondria from AIFM1 knockout cells (Fig 1F and G; Appendix Fig S2B).

The levels of four MIA40/CHCHD4 substrates linked to complexes III and IV were lowered in AIFM1 knockout cells as well (Fig 1C and E). COA5, COA6, and CMC2 are assembly factors of complex IV and do not serve as structural subunits. Their decrease

© 2022 The Authors

to ~ 40–50% of wildtype levels did not delay complex IV assembly sufficiently to reduce the amounts of its subunits (Appendix Fig S2C) or its activity (Appendix Fig S2B). This may indicate that these complex IV assembly factors have a certain reserve capacity in wildtype HEK293 cells. Tissue-specific alterations of such reserve capacities might explain tissue-to-tissue differences previously observed in various *in vivo* models. UQCRH is a structural component of complex III, and its levels were decreased in AIFM1 knockout cells to about 40% of wildtype levels. We did not detect changes in the levels of other complex III subunits (Appendix Fig S2C). Complex III activity tended to be slightly but was not significantly decreased (Appendix Fig S2B).

Collectively our findings demonstrate reduced complex I levels and activity despite normal MIA40/CHCHD4 levels in AIFM1 knockout cells. In contrast, other complexes of the respiratory chain were hardly affected. This indicates the previously observed loss of MIA40/CHCHD4 substrates and complex I in the harlequin mouse or during siRNA-mediated AIFM1 depletion (Hangen *et al*, 2015; Meyer *et al*, 2015) cannot be explained by the loss of mitochondrial MIA40/CHCHD4 alone.

### NDUFS5 is absent from complex I assembly intermediates in AIFM1 knockout HEK293 cells

To address the question of how AIFM1 knockout leads to reduced levels of complex I, we employed complexome profiling analysis (Heide *et al*, 2012; Van Strien *et al*, 2019). To this end, proteins and protein complexes from digitonin-lysed mitochondria were separated on BN–PAGE and analyzed by mass spectrometry after tryptic in-gel digestion and label-free quantification of 60 evenly sized slices cut from the gel (Appendix Fig S3A). Proteins were clustered and the distribution of individual proteins or protein (sub)complexes (as averages of the abundances of their constituent proteins) was visualized as profile plots and heatmaps. Additionally, relative abundances of proteins in mass ranges specific to complexes and subcomplexes were integrated and represented as bar diagrams. Of the 44 different subunits of complex I, only ND4L and NDUFA1 were not detected. The other 42 were present in wildtype cells, AIFM1 knockout cells, and after complementation (Appendix Fig S3A).

In wildtype cells, complex I subunits exhibited their highest abundance at around 1,650 kDa corresponding to respiratory chain supercomplex $S_1$ (respirasome I/$III_2$/IV), which is known to contain essentially all of complex I in human cells. In AIFM1 knockout cells, the supercomplex and thus complex I were diminished to 30–40% of wildtype. Complementation with AIFM1-HA restored complex I levels (Appendix Fig S3B). Notably, the decrease in complex I in the respirasome matched the loss in activity (Fig 1G) indicating that, once completely assembled, complex I is fully functional also in AIFM1 knockout cells. Conversely, levels of the other respiratory chain complexes were not significantly affected (Appendix Fig S3B).

In complex I assembly, individual modules are first assembled and then later on joined in a stepwise fashion (Fig 2A). Hereby, the four MIA40/CHCHD4 substrates in complex I, NDUFA8, NDUFB7, NDUFB10, and NDUFS5 appear at different stages of the assembly pathway. NDUFA8, NDUFB7, and NDUFB10 first appear in the Q/$P_{P\text{-}a}$, $P_{D\text{-}b}$, and $P_{D\text{-}a}$, assembly intermediates, respectively (Fig 2A; Guerrero-Castillo *et al*, 2017, Ugalde *et al*, 2004). NDUFS5 appears in the $P_{P\text{-}b}/P_{D\text{-}a}$ or Q/$P_P$ intermediates (Fig 2A). Importantly, even under unperturbed conditions, complex I assembly intermediates can be identified and quantitatively assessed by complexome profiling thus allowing for specifically assess how AIFM1 knockout affects the assembly pathway (Guerrero-Castillo *et al*, 2017, Heide *et al*, 2012; Appendix Fig S3A).

To identify specific assembly intermediates, we quantified the involved subunits in the respective mass range. Observed changes in AIFM1 knockout cells were largely reversed to wildtype levels following complementation with AIFM1 with or without tag (Appendix Fig S4A–H). Levels of the $P_{D\text{-}a}$, Q/$P_{P\text{-}a}$, and $P_{D\text{-}b}$ assembly intermediates were increased in AIFM1 knockout cells compared with wildtype, while levels of the $P_{P\text{-}b}$ intermediate, the free N-module, and the $P_{P\text{-}b}/P_{D\text{-}a}$ assembly intermediates remained essentially unchanged (Fig 2A; Appendix Fig S4B–G). Only the Q/$P_P$ assembly intermediate was dramatically lowered in abundance (Fig 2A; Appendix Fig S4H). Unexpectedly, however, it appeared

**Figure 2. Absence of AIFM1 stalls complex I assembly likely due to impaired NDUFS5 insertion.**

A The modular assembly pathway of complex I. Simplified model as deduced from (Guerrero-Castillo *et al*, 2017). The MIA40/CHCHD4 substrates NDUFA8, NDUFB7, NDUFB10, and NDUFS5 and their entry during complex I assembly are highlighted in shades of red and labeled omitting the leading "NDUF." In AIFM1 knockout cells, levels of the $P_{D\text{-}a}$, Q/$P_{P\text{-}a}$, $P_{D\text{-}b}$ assembly intermediates, and the Q/P range were increased (green arrows). Levels of the $P_{P\text{-}b}$, free N-module, and $P_{P\text{-}b}/P_{D\text{-}a}$ were not significantly changed (gray arrows). Levels of Q/$P_P$ and complex I were decreased in AIFM1 knockout cells (red arrows). These findings indicate dramatic changes in complex I assembly in AIFM1 *KO* cells and point to specific stalling points (for details see Appendix Figs S3 and S4).

B Bar diagram showing a summary of the detailed analysis of the Q/P range using high-resolution complexome profiling HEK293, AIFM1 knockout, and AIFM1 knockout complemented with AIFM1 or AIFM1-HA (for details, see Appendix Fig S5). $P_{P\text{-}b}/P_{D\text{-}a}$ and the assembly factors MCIA, TMEM70, and TMEM126A were enriched in this range. Their combined mass is, however, only half of the mass indicated by their migration in the Q/P range leading to the hypothesis that a dimer containing $P_{P\text{-}b}/P_{D\text{-}a}$ and the assembly factors accumulates in AIFM1 knockout cells. $N$ = 6 biological replicates, except AIFM1 *KO* + AIFM1 ($N$ = 3); error bars indicate SD and an unpaired, two-sided Student's $t$-test was applied (*$P$ < 0.05, **$P$ < 0.01).

C Bar diagram showing amounts of NDUFB10 and NDUFS5 and the $P_{P\text{-}b}/P_{D\text{-}a}$ assembly intermediate in HEK293, AIFM1 knockout, and AIFM1 knockout complemented with AIFM1 or AIFM1-HA. Data are normalized to the wildtype assembly intermediates (WT = 1). NDUFS5 is missing from $P_{P\text{-}b}/P_{D\text{-}a}$ although the module (and also NDUFB10) is present at normal levels. $N$ = 6 biological replicates, except AIFM1 *KO* + AIFM1 ($N$ = 3); error bars indicate SD and an unpaired, two-sided Student's $t$-test was applied (**$P$ < 0.01, ***$P$ < 0.001, ****$P$ < 0.0001).

D Disulfide relay substrates in complex I. The structure of mammalian complex I (Agip *et al*, 2018) and the positioning of the four disulfide relay substrates NDUFA8, NDUFB7, NDUFB10, and NDUFS5 are shown as viewed from the IMS. Cartoon was prepared from PDB 6G2J using the PyMOL Molecular Graphics System, Version 2.0 (Schrödinger, LLC). Color code of submodules and individual proteins is the same throughout the manuscript. NDUFS5 is positioned below NDUFA8 in mature complex I.

E Model for altered complex I assembly in AIFM1 knockout cells. Complex I assembly stalls at the height of the $P_{P\text{-}b}/P_{D\text{-}a}$ module due to the absence of NDUFS5. This leads to the accumulation of a dimer containing $P_{P\text{-}b}/P_{D\text{-}a}$.


© 2022 The Authors

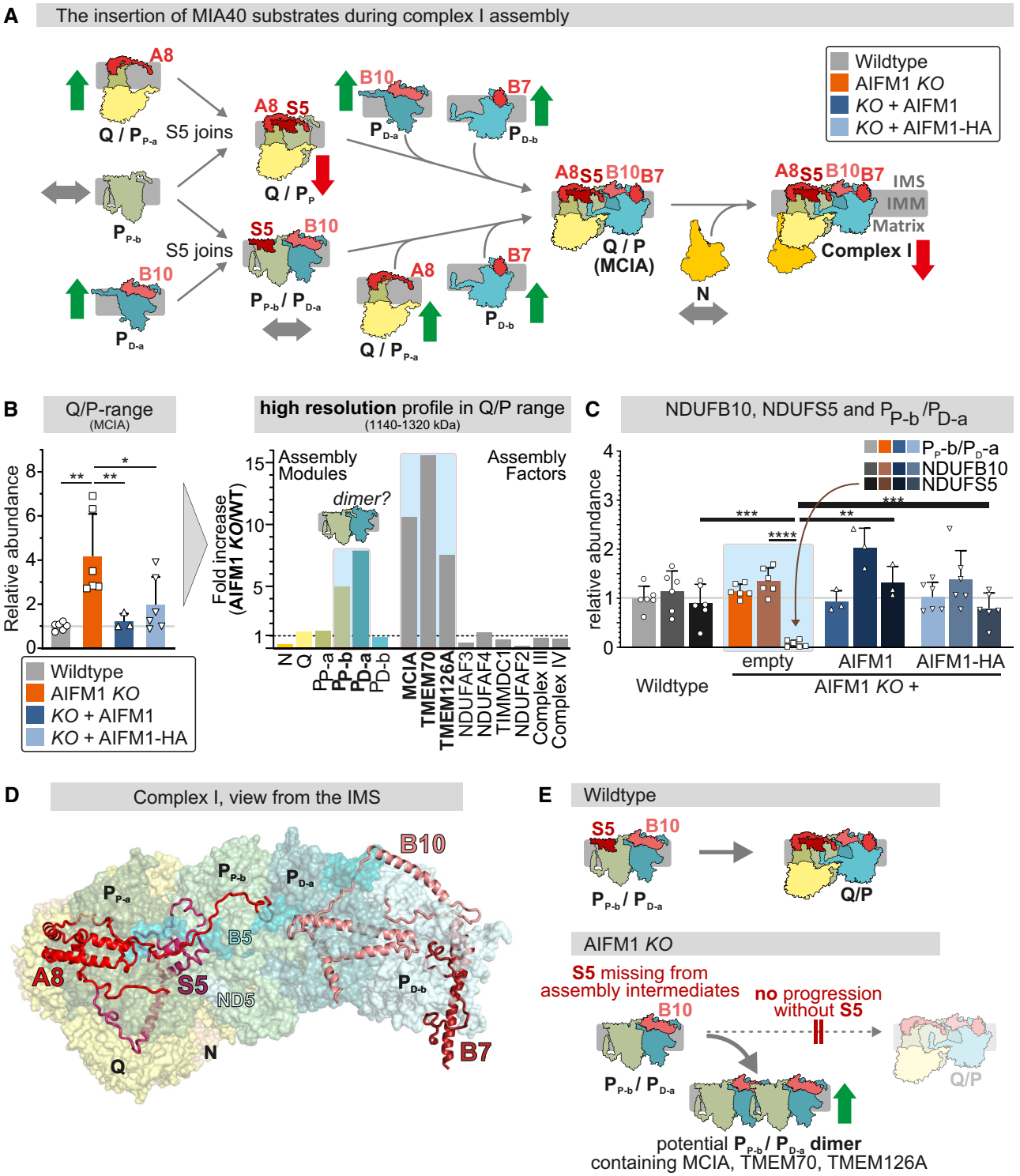



**Figure 2.**

that the subsequent Q/P intermediate was markedly increased in AIFM1 knockout cells (Guerrero-Castillo *et al*, 2017).

Therefore, we performed a more detailed analysis of the intermediates in the mass range > 1 MDa by an additional set of high-resolution complexome profiling experiments that indicated accumulation of an additional, previously not observed, intermediate and excluded accumulation of the Q/P intermediate. This novel intermediate contained the MCIA assembly factors (ACAD9. ECSIT, NDUFAF1, TMEM126), and COA1, TMEM186, and TMEM70 (Appendix Fig S5C). NDUFAF3, NDUFAF4, and TIMMDC1 that are associated with the Q/P module were not present in this novel intermediate (Fig 2B, *right panel*; Appendix Fig S5C).

© 2022 The Authors

Moreover, we observed that subunits of the modules $P_{P\text{-}b}$ and $P_{D\text{-}a}$ in the mass range > 1 MDa were increased in the AIFM1 knockouts as well (Fig 2B, *right panel* and Appendix Fig S5D). From this, we concluded that this novel, likely off-pathway, intermediate might be a dimer of the previously described $P_{P\text{-}b}/P_{D\text{-}a}$ intermediate containing additional assembly factors (Appendix Fig S5E).

Next, we assessed MIA40/CHCHD4 substrate levels in the different assembly intermediates. While NDUFB10, NDUFB7, and NDUFA8 were present in stoichiometric amounts with their assembly intermediates in AIFM1 knockout cells (Appendix Fig S6A–C), NDUFS5 exhibited a distinctly different behavior (Fig 2C; Appendix Fig S6D–F): Of the two first assembly intermediates to which NDUFS5 associates in wildtype cells, the $Q/P_P$ intermediate was almost completely absent, while levels of the $P_{P\text{-}b}/P_{D\text{-}a}$ intermediate were hardly changed. NDUFB10 precisely followed the behavior of the $P_{P\text{-}b}/P_{D\text{-}a}$ intermediate in AIFM1 knockout cells. Conversely, NDUFS5 was absent. NDUFS5 was also not found in the newly detected ~ 1,250 kDa dimeric $P_{P\text{-}b}/P_{D\text{-}a}$ intermediate (Appendix Fig S6F). Finally, it should be noted that NDUFS5, although it associates with this module in mature complex I, is not part of the $P_{P\text{-}b}$ assembly intermediate (Appendix Fig S6D, not even in WT), which was not entirely clear from a previous study (Guerrero-Castillo *et al*, 2017).

Taken together, in AIFM1 knockout cells, NDUFS5 is the only MIA40/CHCHD4 substrate absent from essentially all assembly intermediates containing this subunit in wildtype cells. Our results and the positioning of NDUFS5 in the complex I structure (Fig 2D) indicate that NDUFS5 is critical for the formation of $Q/P_P$-containing intermediates ($Q/P_P$ or Q/P). Its absence in AIFM1 knockout cells reduces complex I assembly by impairing $P_{P\text{-}a}/P_{P\text{-}b}$ association and reroutes this intermediate to a dimeric $P_{P\text{-}b}/P_{D\text{-}a}$/TMEM70/TMEM126A/TMEM186/COA1 complex (Fig 2E), which is not observed in the normal assembly pathway. Notably, in fully assembled complex I, the reduction in NDUFS5 and the other three MIA40/CHCHD4 substrates paralleled the reduction in overall levels of the enzyme (Appendix Fig S6G). This indicates that the availability of NDUFS5 limits the progress of complex I assembly because it is required for the stable formation of the proximal part of its membrane arm. In conclusion, we hypothesize that reduced levels of NDUFS5 lead to complex I deficiency in AIFM1 knockout by impairing late steps of its assembly.

### MIA40/CHCHD4 substrate import and oxidation are impaired in AIFM1 knockout cells

To investigate the cause of low levels of NDUFS5 in AIFM1 deficient cells, we studied its translocation, import, and maturation in cell culture and isolated mitochondria (Fischer *et al*, 2013; Murschall *et al*, 2021). For import assays, *in vitro* translated radioactive precursor proteins are incubated together with mitochondria for different time periods. After the import reaction, nonimported precursor proteins are removed by proteinase K treatment, and mitochondria are analyzed by autoradiography. We analyzed the import of NDUFS5 and as control NDUFB7 (which is structurally most similar to NDUFS5, Fig 3A) into mitochondria isolated from wildtype and AIFM1 knockout cells. We found that loss of AIFM1 resulted in impaired protein import of both, NDUFS5 and NDUFB7. However, NDUFS5 was more severely affected with only 40% of protein imported into mitochondria from AIFM1 knockout cells compared with wildtype mitochondria after 30 min (NDUFB7, 70%; Fig 3A).

To assess NDUFS5 and NDUFB7 maturation in intact cells, we performed pulse-chase oxidation kinetics assays. Hereby, intact cells are radioactively labeled for a short time followed by various nonradioactive chase periods. Subsequently, cells are lysed and free (reduced) thiols but not oxidized thiols are modified by a maleimide derivative that adds mass to the modified protein. Lastly, proteins are immunoprecipitated and analyzed by SDS–PAGE and autoradiography. In AIFM1 knockout cells, we found a delayed occurrence of the oxidized mature forms of NDUFB7 that correlated well with the delayed disappearance of the reduced cytosolic precursor (Fig 3B). Still, after 20 min chase time, NDUFB7 was fully oxidized also in

**Figure 3. NDUFS5 import and oxidation are impaired in AIFM1 knockout.**

A *In organello* import assay with NDUFS5, NDUFB7 and as controlling the matrix protein SOD2. *In vitro* translated radioactive proteins were incubated with mitochondria isolated from HEK293 and AIFM1 knockout cells. Nonimported proteins were removed by treatment with Proteinase K. Imported proteins were analyzed by reducing SDS–PAGE and autoradiography. Signals were quantified using ImageQuantTL and the amount of imported protein was plotted. NDUFS5 import is strongly affected by the loss of AIFM1. Import of NDUFB7 is less affected and SOD2 import remained unaffected. This is despite the fact that the core domains important for oxidative folding of NDUFS5 and NDUFB7 are very similar. $N = 3$ replicates; error bars indicate SD.

B Oxidation kinetics of endogenous NDUFB7 and NDUFS5. HEK293 cells, AIFM1 knockout cells, and AIFM1 knockout cells complemented with AIFM1-HA were analyzed by pulse-chase experiments coupled to redox state determination. To this end, cells were incubated with $^{35}$S-Met for 5 min (pulse). After removal of $^{35}$S-Met, cells were left in "cold" met for different chase times. Further oxidation was stopped by the addition of trichloroacetic acid (TCA). Free thiols but not thiols in disulfide bonds were modified using mmPEG24, and then, MIA40/CHCHD4 substrates were enriched by immunoprecipitation (IP) and analyzed by nonreducing SDS–PAGE and autoradiography. Occurrence of oxidized NDUFB7 was slightly delayed in AIFM1 knockout cells. NDUFS5 levels dropped rapidly and only little oxidized NDUFS5 could be observed. $N = 4$ biological replicates for NDUFB7 and NDUFS5. Error bars indicate SD.

C Synthesis of NDUFS5 and NDUFB7 in wildtype and AIFM1 knockout cells. Cells were incubated with $^{35}$S-Met for 5 min (pulse), and then, MIA40/CHCHD4 substrates were enriched by immunoprecipitation (IP) and analyzed by nonreducing SDS–PAGE and autoradiography. NDUFS5 and NDUFB7 are synthesized in equal amounts in wildtype and AIFM1 knockout cells.

D Interaction between endogenous MIA40/CHCHD4 and its substrates in wildtype and AIFM1 knockout cells. Cells were subjected to native immunoprecipitation (IP) against endogenous MIA40/CHCHD4. Precipitates were analyzed by SDS–PAGE and immunoblotting against the indicated proteins. In AIFM1 knockout cell interaction between MIA40/CHCHD4 and its substrates is strongly affected with the interaction between MIA40/CHCHD4 and NDUFS5 almost completely abolished. This is despite the fact that NDUFS5 and NDUFB7 are synthesized in equal amounts in wildtype and AIFM1 knockout cells, indicating that lowered steady-state levels of these proteins are a consequence of a lacking interaction with MIA40/CHCHD4 rather than the cause. Quantification using Image lab. Data from 2 experiments were combined and standard deviations are presented. Asterisk indicates background band; orange arrow indicates a signal of NDUFS5 and NDUFB7 in AIFM1 KO cells, respectively.


© 2022 The Authors

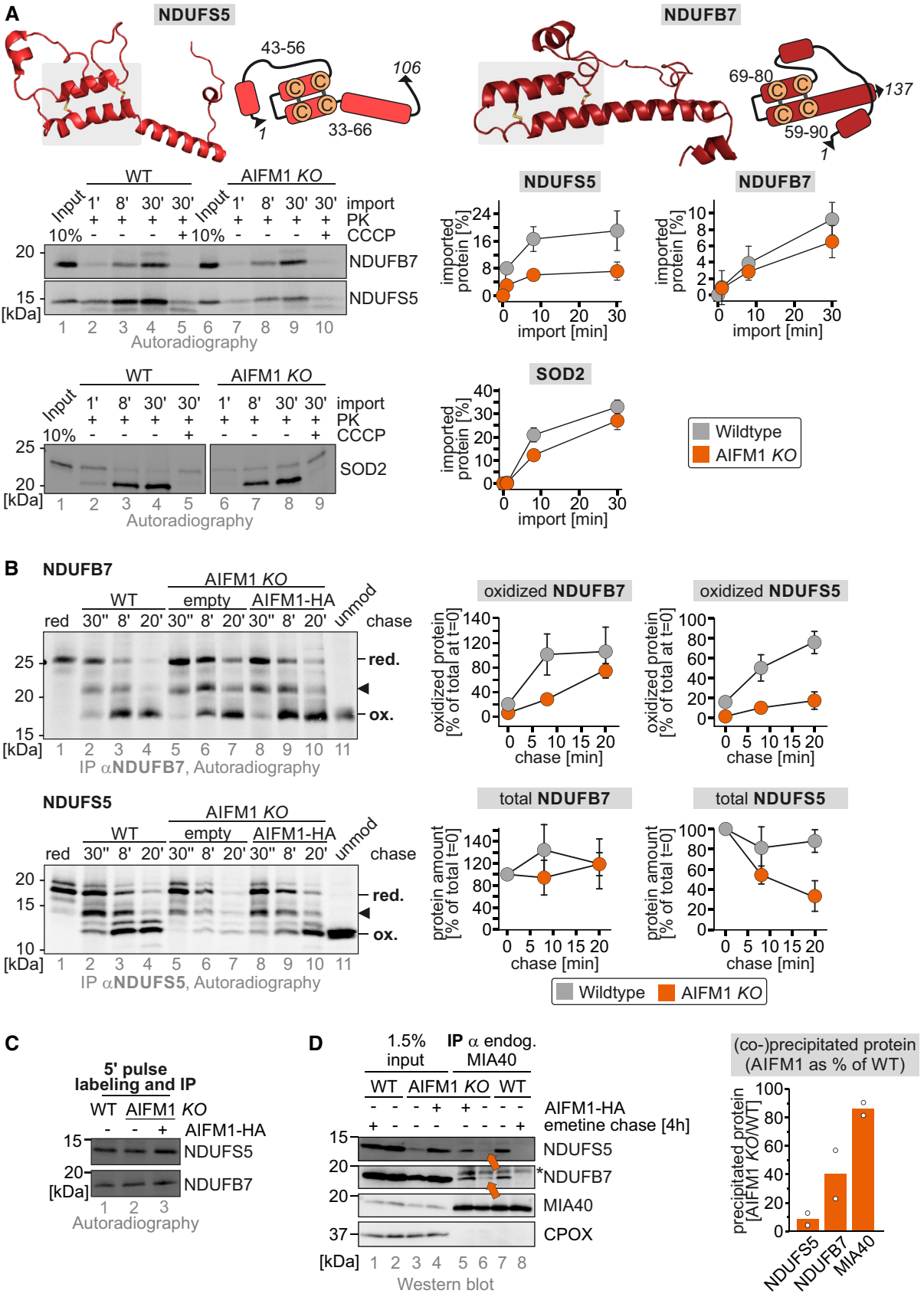



**Figure 3.**

© 2022 The Authors

AIFM1 knockout cells. Since oxidation of NDUFB7 was delayed only to a small extent (and total protein levels remained constant during the chase time), we concluded that the strongly lowered levels of NDUFB7 at steady state (Fig 1C–E) probably were secondary effects resulting from the impaired assembly of complex I and subsequent degradation of assembly intermediates by YME1L (Hangen *et al*, 2015). Conversely, the appearance of oxidized NDUFS5 was strongly delayed in AIFM1 knockout cells; even after 20 min chase time, < 20% of the initially synthesized protein was present in the oxidized form (Fig 3B). Additionally, total amounts of NDUFS5 decayed rapidly (Fig 3B).

For OMM translocation of NDUFS5 and NDUFB7, we assessed their interaction with MIA40/CHCHD4. Since OMM translocation relies on MIA40/CHCHD4 (Peleh *et al*, 2016; Habich *et al*, 2019), immunoprecipitation of endogenous MIA40/CHCHD4 and assessment of coprecipitating substrates can act as a proxy to reveal the efficiency of the translocation process. It is important to note that the MIA40/CHCHD4-substrate interaction takes place early in precursor maturation, and that in the tested cell lines, similar precursor amounts of endogenous NDUFS5 and NDUFB7 were translated as demonstrated by a radioactive pulse assay (Fig 3C).

To compare the efficiency of substrate-MIA40/CHCHD4 interaction between wildtype and AIFM1 knockout cells, we immunoprecipitated endogenous MIA40/CHCHD4 and then analyzed the precipitates. We found that in AIFM1 knockout cells the interaction between MIA40/CHCHD4 and both, NDUFB7 and NDUFS5, was disturbed (Fig 3D, lanes 6 and 7, orange arrows). However, the NDUFS5-MIA40/CHCHD4 interaction appeared to be more drastically affected (Fig 3D, quantification). We would like to point out that the comparison of input and immunoprecipitated signals in this experiment can be misleading. The input reflects steady-state levels of MIA40/CHCHD4 substrates that are lowered due to failed maturation of the substrates and complex I assembly, thus it is rather a consequence of the impaired interaction. The similar precursor amounts detected by pulse analyses (Fig 3C) better reflect the amounts encountered by MIA40/CHCHD4 during substrate translocation.

Thus, in AIFM1 knockout cells, the lack of NDUFS5 indeed appears to be caused by an impaired import and maturation of the protein likely caused by the failure of NDUFS5 to efficiently interact with MIA40/CHCHD4—the prerequisite for OMM translocation.

### AIFM1 and MIA40/CHCHD4 are present in a stable long-lived complex

How does the loss of AIFM1 influence the functionality of the mitochondrial disulfide relay, although MIA40/CHCHD4 levels, localization, and its redox state are unchanged in AIFM1 knockout cells? We hypothesized that in addition to serving as its import receptor, AIFM1 also cooperates with MIA40/CHCHD4 in substrate import, which would imply an extended interaction between both proteins.

To test this, we first confirmed features of the MIA40/CHCHD4-AIFM1 interaction at steady state by immunoprecipitating different MIA40/CHCHD4-Strep variants followed by immunoblot analysis (Fig 4A; Hangen *et al*, 2015): As shown previously, the interaction could be abolished by removing 40 amino acids from the N-terminus of MIA40/CHCHD4 (Δ1-40 MIA40/CHCHD4). However, in contrast to the interaction with its disulfide relay partner ALR, the interaction with AIFM1 could not be reestablished by equipping Δ1-40 MIA40/CHCHD4 with a targeting sequence for the IMS (Fig 4A, lane 9). We also showed that the interaction was independent of the redox-active cysteines in MIA40/CHCHD4 (Appendix Fig S7A and B). Notably, both isoforms of MIA40/CHCHD4 interacted with AIFM1 although they differ at their very N-terminus (Appendix Fig S7C).

Next, we tested for the dynamics of the MIA40/CHCHD4-AIFM1 interaction in intact cells. To this end, we performed immunoprecipitation experiments after incubation of cells with the ribosome inhibitor emetine. We found that even after 6–8 h of emetine treatment, a time well beyond the time needed for MIA40/CHCHD4 maturation (half time of import approx. 60–90 min; Murschall *et al*, 2020), AIFM1 coprecipitated with MIA40/CHCHD4 and *vice versa* (Fig 4B and C). Corroborating these findings, MIA40/CHCHD4 interacted during the entire chase time with AIFM1 in a pulse-chase experiment in which we labeled cells radioactively and then followed the fate of the MIA40/CHCHD4-AIFM1 interaction by immunoprecipitation (Appendix Fig S7D).

To complement our immunoprecipitation-based interaction studies, we reconstituted the AIFM1-MIA40/CHCHD4 complex

**Figure 4. MIA40/CHCHD4 is present in a stable long-lived complex with AIFM1.**

A Assessment of MIA40/CHCHD4 variant-AIFM1 interaction. The indicated MIA40/CHCHD4-Strep variants were affinity precipitated (AP) under native conditions after stopping thiol-disulfide exchange reactions by NEM incubation. Precipitates were tested for AIFM1, ALR, and MIA40/CHCHD4 by reducing SDS–PAGE and immunoblotting. 1% of the total lysate was loaded as input control. M, mock control not expressing MIA40-Strep. Both, wildtype MIA40/CHCHD4 and MTS-MIA40/CHCHD4 but not MIA40/CHCHD4$^{\Delta 1-40}$ variants coprecipitated AIFM1. All mitochondria-localized variants precipitate ALR indicating redox functionality. Arrowhead indicates endogenous MIA40/CHCHD4.

B, C Emetine-chase experiments to assess the stability of the AIFM1/CHCHD4 complex. HEK293 cells stably expressing MIA40/CHCHD4-Strep (B) or AIFM1 knockout cells stably expressing AIFM1-HA (C) were treated for the indicated times with the ribosome inhibitor emetine. Then, cells were lysed under native conditions (Triton X-100), and MIA40/CHCHD4-Strep (B) or AIFM1-HA (C) were precipitated. Precipitates were analyzed by reducing SDS–PAGE and immunoblotting. MIA40/CHCHD4 and AIFM1 interact over a period of at least 6–8 h (B, C), while the two MIA40/CHCHD4 substrates, NDUFB7 and AK2, are quickly released from MIA40/CHCHD4 (B, gray box). AP, affinity precipitation; asterisk, background band. *N* = 3 biological replicates.

D, E Gel filtration analysis to assess the *in vitro* reconstituted AIFM1-MIA40/CHCHD4 complex. Purified MIA40/CHCHD4 and AIFM1 were incubated in the presence of NADH and subjected to gel filtration analysis. Elution was monitored by following the absorption at 280 nm (D). Eluted fractions were subjected to SDS–PAGE and TCE staining (E). AIFM1 and full-length MIA40/CHCHD4 migrate together indicating the formation of a complex. MIA40/CHCHD4 was present in excess over AIFM1 resulting in the presence of free MIA40/CHCHD4. AIFM1 and Δ1-40 MIA40/CHCHD4 do not migrate together emphasizing the importance of the N-terminal amino acids in MIA40 for interaction with AIFM1.

F Isothermal Titration Calorimetry (ITC) analysis of AIFM1 and MIA40/CHCHD4. The partners bind to each other with a $K_D$ of approximately 0.18 μM and stoichiometry between AIFM1 and MIA40/CHCHD4 of 2 to 1. Data shown were normalized by the background signal of titrating MIA40/CHCHD4 into the buffer.


© 2022 The Authors

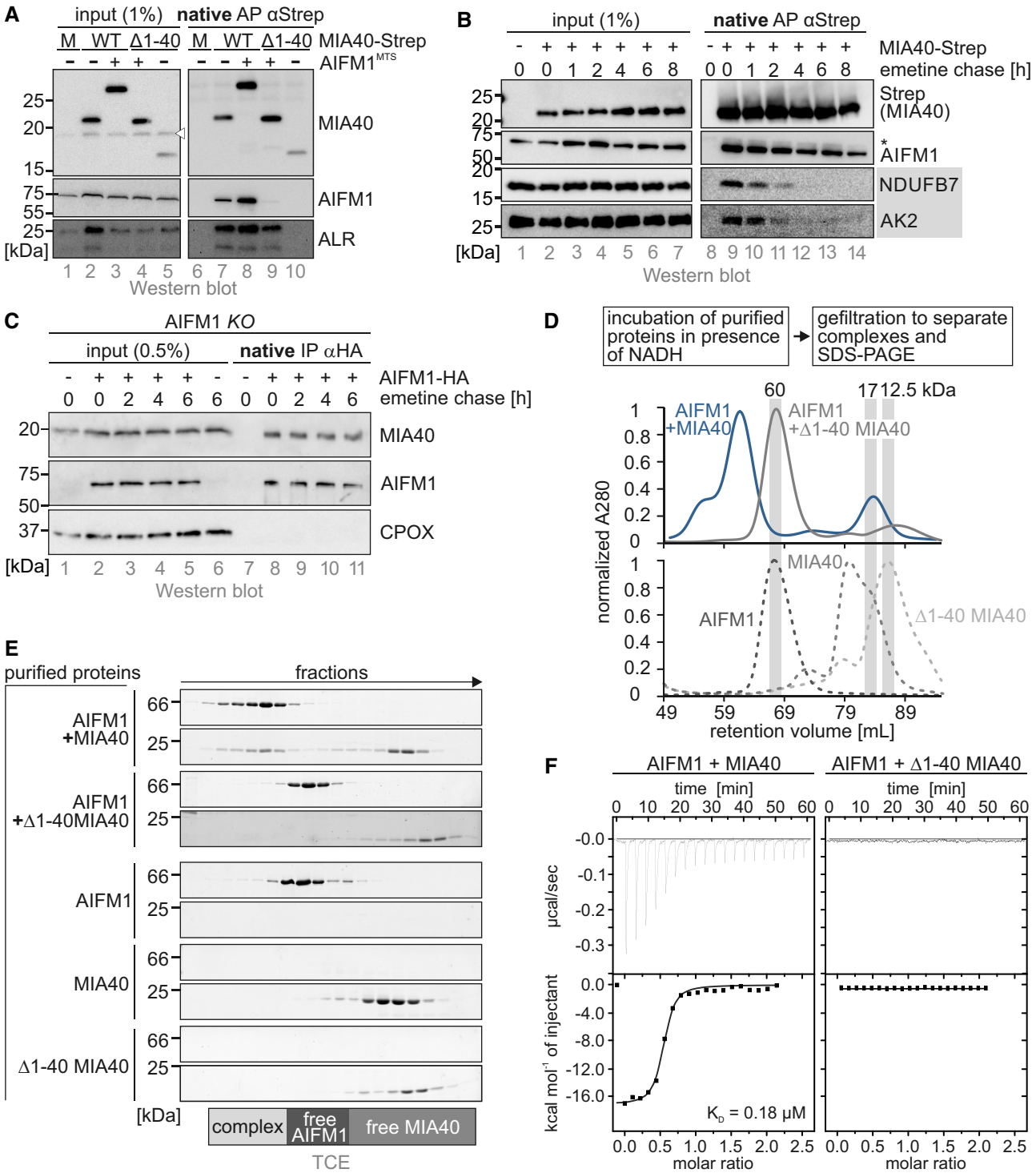



**Figure 4.**

*in vitro*. To this end, we purified AIFM1 without its transmembrane domain and incubated it in presence of NADH either with purified full-length MIA40/CHCHD4, with purified Δ1-40 MIA40/CHCHD4, or with a peptide representing the stretch between amino acids 7 and 28 of MIA40/CHCHD4 isoform 1 that in a previous study was sufficient to establish this interaction (Hangen *et al*, 2015; Appendix Fig S8A–D).

We subjected the protein mixtures to gel filtration, monitored the absorption of the elution fractions at 280 nm (Fig 4D), and analyzed individual fractions by SDS–PAGE (Fig 4E). We found that AIFM1 and full-length MIA40/CHCHD4 co-migrated. AIFM1 incubated with Δ1-40 MIA40/CHCHD4 migrated like AIFM1 alone indicating no interaction between these proteins (Fig 4D and E). We confirmed the stable NAD(P)H-dependent interaction between AIFM1 and the

© 2022 The Authors

N-terminal region of MIA40/CHCHD4 using the MIA40/CHCHD4 peptide in a fluorescence-based binding assay (Appendix Fig S8E–J).

To further quantitatively assess the interaction between AIFM1 and MIA40/CHCHD4, we performed Isothermal Titration Calorimetry (ITC; Fig. 4F). We thereby determined dissociation constant of 0.18 μM, and a stoichiometry of two AIFM1 molecules to one MIA40/CHCHD4 indicating that the AIFM1 dimer binds one MIA40 molecule. In contrast to full-length MIA40/CHCHD4, the dissociation constant of the AIFM1-CHCHD4/MIA40 peptide interaction was an order of magnitude higher ($K_D$ = 2.94 μM, Appendix Fig S8K) indicating that other regions in MIA40/CHCHD4 might contribute to binding strength. Our findings are in line with previous results (Hangen *et al*, 2015; Romero-Tamayo *et al*, 2021) and extend them by showing that MIA40/CHCHD4 and AIFM1 form a stable long-lived complex with a 1-to-2 stoichiometry in the presence of NAD(P)H.

### The majority of MIA40/CHCHD4 in the cell is bound to AIFM1

Next, we characterized the AIFM1-MIA40/CHCHD4 complex in intact cells (Fig 5). First, we lysed HEK293 cells in a native lysis buffer containing the detergent Triton X-100, subjected the cleared lysate to gel filtration and then analyzed individual fractions by immunoblotting. We found that endogenous AIFM1 and MIA40/CHCHD4 co-migrated in a broad peak with a size above 150 kDa as judged by comparison to control proteins (Fig 5A). Notably, we detected only minute amounts of MIA40/CHCHD4 in the lower molecular mass range.

Then, we tested how the migration of the AIFM1-MIA40/CHCHD4 complex was influenced by modulation of AIFM1 and MIA40/CHCHD4 levels, respectively. Both, siRNA-mediated loss of AIFM1 and AIFM1 knockout, led to MIA40/CHCHD4 migrating at an apparent mass of just above 30 kDa (Fig 5A and Appendix Fig S9A). Conversely, decreasing MIA40/CHCHD4 levels led only to a small size shift of the AIFM1 fraction (Appendix Fig S9A and B). Overexpression of MIA40/CHCHD4 led again to the accumulation of MIA40/CHCHD4 at 30 kDa indicating that in HEK293 cells, AIFM1 and MIA40/CHCHD4 normally are present in carefully balanced amounts (Appendix Fig S9C). Lastly, expression of Δ1-40 MIA40/CHCHD4-Strep resulted in the accumulation of its monomeric form indicating again the necessity of the N-terminal region for the formation of the AIFM1-MIA40/CHCHD4 complex (Fig 5B).

Quantification of these results revealed that in HEK293 cells under unperturbed conditions > 90% of MIA40/CHCHD4 was in a long-lived complex with AIFM1 (Fig 5C). Perturbation of the stoichiometric ratio between AIFM1 and MIA40/CHCHD4 (especially the knockout of AIFM1) led to the accumulation of presumably monomeric MIA40/CHCHD4.

To explore whether our findings apply more generally, we checked different mouse tissues and HepG2 cells for the existence of the MIA40/CHCHD4-AIFM1 complex. The protein levels of AIFM1 and MIA40/CHCHD4 vary between different mouse tissues with most analyzed tissues containing more AIFM1 than MIA40/CHCHD4 compared to that of HEK293 cells (Fig 5D). Still, in Triton-X100 lysed isolated mitochondria from mouse brain, liver, and kidney, and in HepG2 cells the AIFM1-MIA40/CHCHD4 complex was found at similar positions in gel filtration with some of MIA40/CHDH4 and AIFM1 migrating at lower molecular masses consistent with their free forms (Fig 5E). While almost all MIA40/CHCHD4 was found in the complex, the amount of excess AIFM1 varied depending on the tissue and cell type (Fig 5E).

By virtue of its permanent interaction with the membrane protein AIFM1, MIA40/CHCHD4 should be membrane-associated. We assessed the solubility of MIA40/CHCHD4 by isolating mitochondria from wildtype and AIFM1 knockout cell lines and opening the outer membrane by hypoxic swelling. MIA40/CHCHD4 remained bound

**Figure 5. The AIFM1-MIA40/CHCHD4 complex exists ubiquitously and serves in associating MIA40/CHCHD4 with the inner membrane.**

A Gel filtration analysis to assess the AIFM1-MIA40 complex in HEK293 cells. HEK293 cells, cells lacking AIFM1 (AIFM1 knockout, AIFM1 *KO*), or AIFM1 knockout cells complemented with AIFM1-HA were lysed under native conditions (Triton X-100), and the cleared lysates subjected to gel filtration analysis. Eluted fractions were subjected to TCA precipitation, resuspension in loading buffer containing SDS and DTT, and subsequent immunoblotting against AIFM1 and MIA40. Endogenous AIFM1 and all endogenous MIA40 migrate in a complex with a size larger than 150 kDa (as judged by comparison to protein markers: apoferritin 443 kDa; β-amylase 200 kDa; alcohol dehydrogenase 150 kDa; bovine serum albumin 66 kDa; carbonic anhydrase 29 kDa). Absence of AIFM1 results in the migration of MIA40 at the height of monomeric MIA40. This behavior is partially rescued by complementation with AIFM1-HA. For a number of biological replicates and quantifications, see 5C.

B Gel filtration analysis of a MIA40 variant lacking the first 40 amino acids (Δ1-40 MIA40/CHCHD4-Strep), which constitute the AIFM1 interaction motif. Experiment was performed as described in (A). AIFM1 and endogenous MIA40/CHCHD4 migrate in a complex with a size larger than 150 kDa, while N-terminally truncated MIA40/CHCHD4 migrates as a monomer. For a number of biological replicates and quantifications, see 5C.

C Quantification of 5A,B and Appendix Fig S9. Quantification of the areas representing the region of monomeric MIA40/CHCHD4 and the AIFM1-MIA40/CHCHD4 complex, respectively, was performed. Quantifications consistently show that AIFM1 knockout, siRNA-mediated depletion of AIFM1, and overexpression of MIA40/CHCHD4 all resulted in an increase in monomeric MIA40/CHCHD4 indicating that the amounts of available AIFM1 with respect to the amounts of MIA40/CHCHD4 are tightly regulated. The numbers below the bars indicate the numbers of biological replicates performed. Averages and standard deviations are presented.

D Levels of AIFM1 and MIA40/CHCHD4 in mitochondria isolated from the indicated tissues. Ratio of AIFM and MIA40/CHCHD4 was formed and normalized to ratio in HEK293 cells (= 1). AIFM1 is in the liver and kidney more abundant than MIA40/CHCHD4.

E Gel filtration analysis of lysates prepared from mitochondria isolated from the indicated tissues and from HepG2 and HEK293 cells. Experiment was performed as described in (A). AIFM1 and MIA40/CHCHD4 co-migrate in all samples. Excess AIFM1 migrates at a lower molecular mass. Number of biological replicates in quantification plot. Where appropriate, standard deviations are presented.

F Assessing the solubility of MIA40/CHCHD4 in the IMS. Mitochondria were isolated from the indicated cell lines, and the outer membrane destroyed by hypoxic swelling. MIA40/CHCHD4 remains bound to these mitoplasts when they were isolated from wildtype cells or AIFM1 knockout cells that had been complemented with AIFM1-HA. It was released from cells lacking AIFM1. This indicates that MIA40/CHCHD4 in wildtype cells is membrane-associated via AIFM1.

G Model. Almost all cellular MIA40/CHCHD4 exists in a permanent complex with AIFM1. ALR is not part of the complex. Being in this complex renders MIA40/CHCHD4 membrane-associated. In AIFM1 knockout cells, MIA40/CHCHD4 is present as a soluble monomeric protein.


© 2022 The Authors

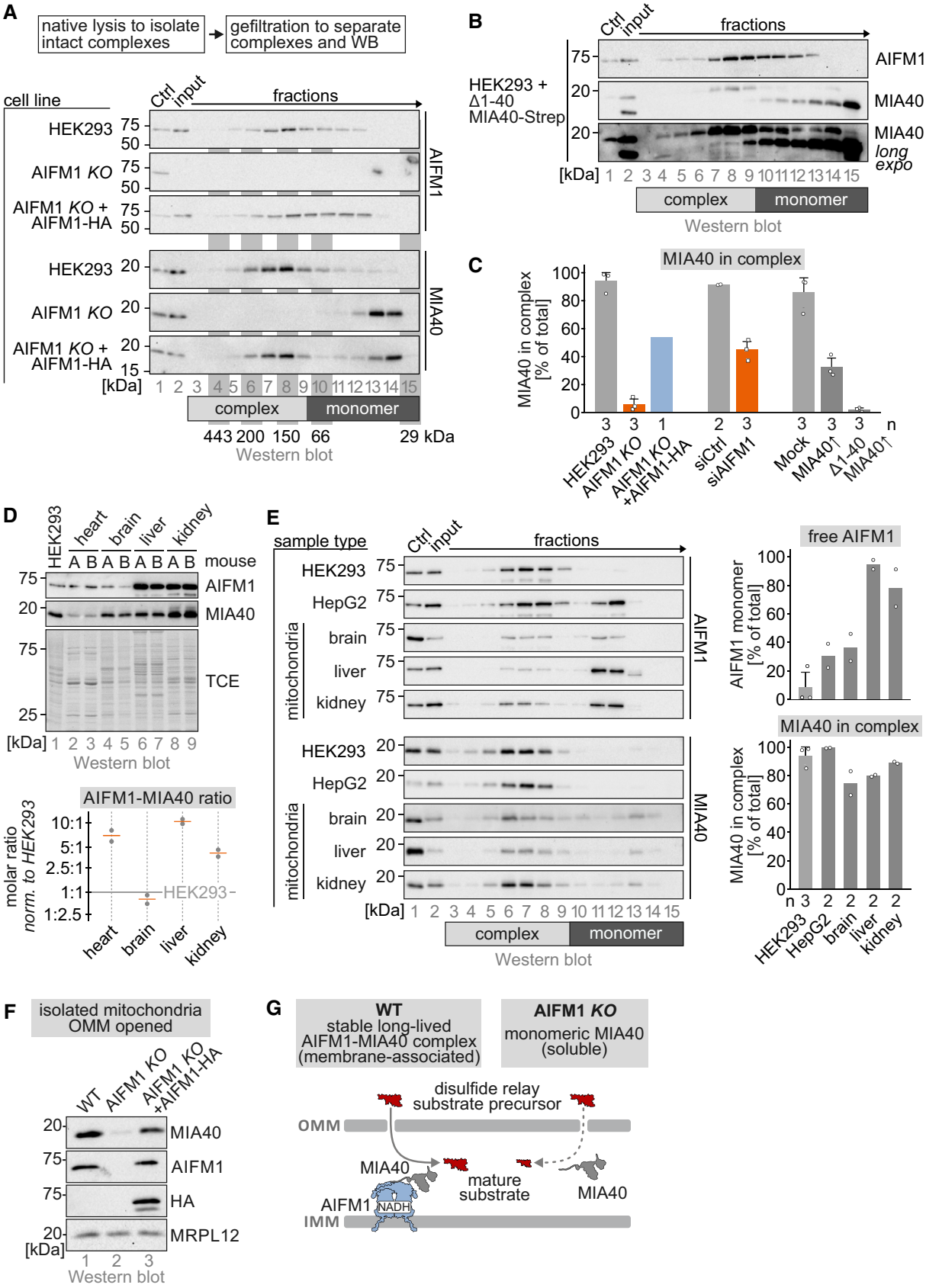

A
native lysis to isolate intact complexes
gefiltration to separate complexes and WB
cell line
Ctrl
input
fractions
HEK293
AIFM1 KO
AIFM1 KO + AIFM1-HA
AIFM1
MIA40
[kDa]
complex
monomer
443 200 150 66 29 kDa
Western blot
B
HEK293 + Δ1-40 MIA40-Strep
AIFM1
MIA40
MIA40 long expo
complex
monomer
Western blot
C
MIA40 in complex
MIA40 in complex [% of total]
HEK293
AIFM1 KO
AIFM1 KO +AIFM1-HA
siCtrl
siAIFM1
Mock
MIA40↑
Δ1-40 MIA40↑
n
D
HEK293
heart
brain
liver
kidney
mouse
AIFM1
MIA40
TCE
Western blot
AIFM1-MIA40 ratio
molar ratio norm. to HEK293
10:1
5:1
2.5:1
1:1
1:2.5
HEK293
E
sample type
HepG2
mitochondria
Western blot
free AIFM1
AIFM1 monomer [% of total]
MIA40 in complex
F
isolated mitochondria
OMM opened
WT
AIFM1 KO
AIFM1 KO +AIFM1-HA
MRPL12
G
WT
stable long-lived AIFM1-MIA40 complex (membrane-associated)
AIFM1 KO
monomeric MIA40 (soluble)
disulfide relay substrate precursor
OMM
MIA40
mature substrate
AIFM1
NADH
IMM

**Figure 5.**

to these mitoplasts when they were isolated from wildtype cells or AIFM1 knockout cells that had been complemented with AIFM1-HA. It was released from cells lacking AIFM1 indicating that in AIFM1 knockout cells MIA40/CHCHD4 is present as soluble IMS protein (Fig 5F).

Collectively, we found that the majority of cellular MIA40/CHCHD4 exists in a complex with AIFM1. Being in this complex renders MIA40/CHCHD4 membrane-associated. In AIFM1 knockout cells, MIA40/CHCHD4 is present as a soluble monomeric protein (Fig 5G).

### In AIFM1 knockout cells NDUFS5 is rapidly degraded by the proteasome

We have previously shown that MIA40/CHCHD4 substrates failing to become imported undergo a redox quality control process (Habich *et al*, 2019; Mohanraj *et al*, 2019). Thereby substrates "slip out" of the TOM pore and become degraded by the proteasome. We thus tested whether the loss of the cytosolic precursor of NDUFS5 in the AIFM1 knockout cells (Fig 3B) depended on the proteasome. Using the pulse-chase MIA40/CHCHD4 substrate maturation assay, we found that the proteasome inhibitor MG132 effectively stabilized the NDUFS5 precursor indicating its degradation in a proteasome-dependent manner in AIFM1 knockout cells (Fig 6A). Nonimported reduced NDUFB7 precursor was not affected by MG132 treatment (Fig 6A). Cytosolic stabilization of NDUFS5 partly increased the amount of oxidized protein after a 20 min chase, but in contrast to wildtype, the majority persisted as a reduced precursor. This indicated that in AIFM1 knockout cells, oxidation-dependent import of NDUFS5 is strongly impaired and not just delayed.

Taken together, NDUFS5 interaction with MIA40/CHCHD4 is impaired in AIFM1 knockout cells. As a consequence, import and oxidation of NDUFS5 are blocked, and the protein is rapidly degraded by the proteasome. Lack of NDUFS5 results in stalling of complex I assembly at specific assembly intermediates (Fig 6B). In wildtype cells, the presence of MIA40/CHCHD4 in a long-lived and stable complex enables the efficient translocation of substrates presumably because for some substrates like NDUFS5 this complex is particularly important due to for example the localization of MIA40/CHCHD4 close to the OMM by AIFM1.

## Discussion

### AIFM1 is a critical component of the mitochondrial disulfide relay

We have demonstrated the presence of a permanent stable complex between MIA40/CHCHD4 and an AIFM1 dimer rendering AIFM1 an integral part of the mitochondrial disulfide relay. In HEK293 and HepG2 cells and in different tissues, most of MIA40/CHCHD4 seems to be confined to the AIFM1-MIA40/CHCHD4 complex. Lowering the levels of AIFM1 resulted in the accumulation of monomeric MIA40/CHCHD4. In human HepG2 cells and mouse tissues, AIFM1 is present in higher amounts than MIA40/CHCHD4 (Wang *et al*, 2019). In these cells, excess AIFM1 is found outside of the AIFM1-MIA40/CHCHD4 complex. It is tempting to speculate that in these cells differential regulation of MIA40/CHCHD4 levels might be sufficient to increase levels of the AIFM1-MIA40/CHCHD4 complex and thereby import rates of specific substrates, explaining how MIA40/CHCHD4 overexpression can improve IMS protein import (Habich *et al*, 2019).

Remarkably, MIA40/CHCHD4 levels were normal in AIFM1 knockout HEK293 cells (Fig 1). This is in contrast to acute depletion of AIFM1 by siRNA and patient samples (Hangen *et al*, 2015; Meyer *et al*, 2015). Here, the loss of MIA40/CHCHD4 was explained by its dependence on AIFM1 for its mitochondrial import. Interestingly, harlequin mice of different ages contained similarly low levels of AIFM1 but varying levels of MIA40/CHCHD4 (Meyer *et al*, 2015; Wischhof *et al*, 2018). This may point to an adaptive mechanism allowing MIA40 import, oxidation, and stabilization even if this import is marginally delayed (Appendix Fig S1B). In AIFM1 knockout cells MIA40/CHCHD4 is probably fully imported by itself, as has been shown for human MIA40/CHCHD4 expressed in yeast cells, which do not harbor AIFM1 (Chacinska *et al*, 2008). Since MIA40/CHCHD4 levels were normal in AIFM1 knockout HEK293 cells, but levels of selected substrates were still decreased, the role of AIFM1 has to extend beyond a mere import receptor function for MIA40/CHCHD4, as previously proposed (Hangen *et al*, 2015). Based on our findings, we thus suggest that AIFM1 serves two overlapping functions: importing (at least to some extent) MIA40/CHCHD4, and constituting an integral part of the disulfide relay that seems to be specific for certain substrates especially those found in complex I.

The presence of AIFM1 in the AIFM1-MIA40/CHCHD4 complex is not essential as its partial or complete loss can be fully complemented by the overexpression of wildtype MIA40/CHCHD4 or a MIA40/CHCHD4 variant bearing an MTS for IMS import (Appendix Fig S10; Hangen *et al*, 2015, Meyer *et al*, 2015). The fact that in AIFM1 knockout cells, the MIA40/CHCHD4 redox state is unchanged and only some MIA40/CHCHD4 substrates are affected, excludes dysfunctional MIA40/CHCHD4 as the cause for slow oxidation of these selected substrates. Rather, our data suggest that AIFM1 is important to allow efficient interaction between MIA40/CHCHD4 and some of its substrates, which is critical for translocation across the OMM. The precise underlying mechanism and why AIFM1 is only critical for some substrates remains to be clarified. Maintaining high import efficiency might be especially important for disulfide relay substrates, which are closely surveilled by quality control systems during import. Recent reports indicate that proteins requiring too long for import are selectively removed by the proteasome (Habich *et al*, 2019; Mohanraj *et al*, 2019). Accordingly, we could partially stabilize substrates by proteasomal inhibition (Fig 6A). However, this did not significantly rescue the AIFM1 knockout phenotype as proteins accumulated as reduced precursors in the cytosol rather than being imported.

Our findings may be indicative of a regulatory mechanism of disulfide relay-dependent import in which the formation of the AIFM1-MIA40/CHCHD4 complex relies on AIFM1 dimerization, which in turn requires NADH binding by AIFM1 (Hangen *et al*, 2015; Appendix Fig S8). NADH is slowly oxidized by AIFM1 using ubiquinone as electron acceptor (Elguindy & Nakamaru-Ogiso, 2015). Shifts in the NADH/$NAD^+$ or ubiquinone/ubiquinol ratios could thereby modulate dimerization of AIFM1 and thus control the level of AIFM1-MIA40/CHCHD4 complex, which in turn would affect the kinetics of disulfide relay-mediated protein import. Such a mechanism would provide a rationale for direct coupling of

 © 2022 The Authors

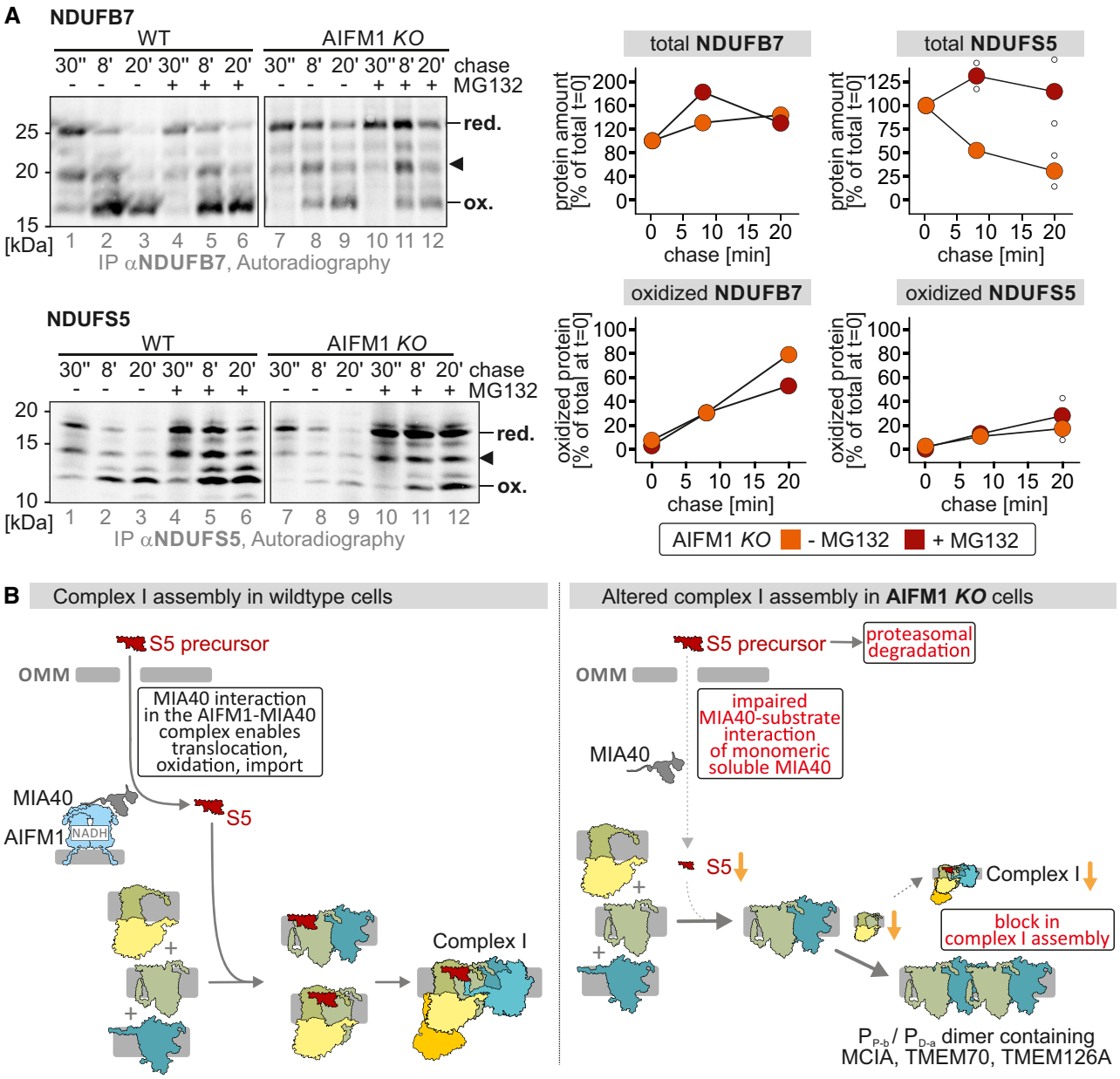



**Figure 6. In AIFM1 knockout cells, impaired OMM translocation of NDUFS5 results in its rapid proteasomal degradation.**

A Oxidation kinetics of NDUFB7 and NDUFS5 in the presence of the proteasome inhibitor MG132. HEK293 cells, AIFM1 knockout cells, and AIFM1 knockout cells complemented with AIFM1-HA were analyzed by pulse-chase experiments coupled to redox state determination. Levels and occurrence of oxidized NDUFB7 were not changed in the presence of MG132. Conversely, NDUFS5 levels were strongly increased. In AIFM1 knockout cells, large amounts of NDUFS5 accumulated in their reduced state indicating impaired oxidation-dependent protein import. The fraction of oxidized protein accumulating is slightly larger than in the absence of MG132. $N = 1$ biological replicate for NDUFB7 and 2 biological replicates for NDUFS5.

B Model. The AIFM1-MIA40/CHCHD4 complex mediates proper oxidation-dependent protein import and insertion of the four disulfide relay substrates into complex I. In the absence of AIFM1, monomeric soluble MIA40/CHCHD4 is still capable of importing many of its substrates. It fails, however, to accumulate NDUFS5. This protein is not properly oxidized and as a consequence, it becomes rapidly degraded by the proteasome. Lack of NDUFS5 results in stalling of complex I assembly and lowered levels of complex I.

IMS protein import to the metabolic state of mitochondria via short-term posttranslational regulation of mitochondrial import. Precursors of the pathway that are not prone to proteasomal degradation would remain import-competent in the cytosol, while others would become rapidly degraded.

### The AIFM1-MIA40/CHCHD4 complex is critical for a specific step of complex I assembly

The loss of the AIFM1-MIA40/CHCHD4 complex elicits a strong effect on complex I but not on complexes III and IV in AIFM1

© 2022 The Authors

knockout HEK293 cells. Despite the fact that complex IV levels are affected in different AIFM1-deficient models (Joza *et al*, 2005; Pospisilik *et al*, 2007; Murari *et al*, 2020), this fits to previously observed tissue-specific effects of AIFM1 deficiency. For example, muscle-specific AIFM1 knockout has been demonstrated to result in reduced complex I and IV levels, while knockout in the liver led to complex I and V reduction (Pospisilik *et al*, 2007). A possible explanation for normal complex IV levels and activity despite AIFM1 loss might be that the complex IV assembly factors that are present in reduced amounts (Fig 1E) are in wildtype HEK293 cells present with a large reserve capacity and thus their reduction by slightly more than half does not affect complex IV assembly.

With our complexome profiling analysis, we were able to mechanistically explain the complex I defect and stage complex I assembly from the viewpoint of the mitochondrial disulfide relay. We confirmed the entry of NDUFA8, NDUFB7, and NDUFB10 with assembly intermediates Q/$P_{P\text{-}a}$, $P_{D\text{-}b}$, and $P_{D\text{-}a}$, respectively (Appendix Fig S6; Guerrero-Castillo *et al*, 2017) and clarified the entry of NDUFS5 at the level of the $P_{P\text{-}b}$/$P_{D\text{-}a}$ and alternatively, the Q/$P_P$ complexes. In AIFM1 knockout cells, we found import and oxidation of NDUFS5 to be impaired. Consequently, NDUFS5 was lacking in all assembly intermediates, and accumulation of a dimeric $P_{D\text{-}a}$/$P_{P\text{-}b}$/TMEM70/TMEM126A/TMEM186/COA1 complex was observed. Apparently, the association of $P_{P\text{-}a}$ with $P_{P\text{-}b}$ was strongly delayed. However, when NDUFS5 eventually enters the complex, progression to fully assembled complex I took place normally, still allowing for steady-state levels of about 30–40% of complex I in AIFM1 knockout cells as compared to wildtype.

No high-resolution structures of any of the complex I assembly intermediates have been solved, but the positioning of NDUFS5 in the structure of mature mammalian complex I (Zhu *et al*, 2016; Agip *et al*, 2018) provides important clues corroborating a critical role in complex I assembly for this subunit (Fig 2D): NDUFS5 is located at the interface between submodules $P_{P\text{-}a}$ and $P_{P\text{-}b}$, i.e., exactly where Q/$P_{P\text{-}a}$ connects to the remainder of the membrane arm. However, NDUFS5 not only binds to the $P_{P\text{-}b}$ module but exhibits several remarkable interactions with other subunits of the membrane arm of complex I. Its extended C-terminus interacts extensively with $P_{P\text{-}a}$, thereby bridging and connecting the two proximal submodules. Vice versa, the C-terminal extension of NDUFA8, a constituent of the $P_{P\text{-}a}$ module, extends to the $P_{P\text{-}b}$ module, where it lies on top of NDUFS5 thereby clamping the Q/$P_{P\text{-}a}$ domain to the remainder of the membrane arm. Moreover, the N-terminus of NDUFS5 is wrapped around the C-terminus of NDUFB5, a subunit of the $P_{D\text{-}a}$ module that extends towards the proximal part of the membrane arm with its C-terminal domain. Finally, NDUFS5 resides adjacent to the C-terminal end of the helix of ND5, the central protein of the $P_{D\text{-}b}$ module, which anchors its unique lateral helix to the membrane arm. Thus, NDUFS5 interacts with components of all four submodules of the membrane arm and may be critical for joining and stabilizing their interaction. In fact, NDUFS5 could be considered as the copestone completing assembly of the membrane arm by joining the critical $P_{P\text{-}a}$/$P_{P\text{-}b}$ interface.

In conclusion, AIFM1 is *per se* not essential for complex I formation. Instead, it appears to take the role of "kinetic accelerator" by maintaining normal NDUFS5 levels. Supporting this notion, MIA40/CHCHD4 overexpression rescued the AIFM1 knockout phenotype. This indicates that MIA40/CHCHD4 alone can take over the function of AIFM1. Since we never observed any association between MIA40/CHCHD4 and any other complex I subunit except for its direct substrates (even under native conditions), we deem it unlikely that under normal conditions MIA40/CHCHD4 acts directly as complex I assembly factor. We thus propose that the AIFM1-MIA40/CHCHD4 complex fulfills its role mainly in disulfide relay substrate oxidation and import and that the strong phenotype in complex I assembly is mainly due to the impaired oxidation and consequent rapid degradation of one structural subunit of complex I, NDUFS5. Collectively, our findings emphasize the role of AIFM1 as a critical component of the mitochondrial disulfide relay.

## Materials and Methods

### Plasmids and cell lines

For plasmids, cell lines, primers, and antibodies used in this study, see Appendix Tables S1–S4, respectively. For the generation of stable, inducible cell lines either the Flp-In T-REx system (Invitrogen) was used in the HEK293 cell line–based Flp-In T-REx-293 cell lines or the Piggy Bac Transposon system (System Biosciences, BioCat) for all further stable, inducible cell lines. HeLa cells were used for siRNA-mediated knockdown experiments. Cells were cultured in DMEM supplemented with 8% fetal bovine serum and penicillin/streptomycin antibiotic mixture at 37°C under 5% $CO_2$.

### Generation of AIFM1 knockout cells

AIFM1 knockout HEK293T cell lines were generated using the pSpCas9(BB)-2A-GFP (PX458) CRISPR/Cas9 construct (a gift from F. Zhang; Addgene, plasmid 4813; Ran *et al*, 2013) as described previously (Stroud *et al*, 2016). In brief, CRISPR/Cas9 gRNAs were designed for gene disruption using CHOPCHOP software (Montague *et al*, 2014). Transfections were performed using Lipofectamine LTX (Thermo Fisher Scientific) and green fluorescent cells were individually sorted. Genomic DNA was isolated from each cell line and the targeted region amplified. PCR products were ligated into pGEM4Z expression vectors and single clones were analyzed by Sanger sequencing.

### Cell treatments

Cells were cultivated with a medium supplemented with the proteasomal inhibitor MG132 (in DMSO) in a concentration of either 1 μM for 16 h or 5 μM for 4 h, for western blot analysis. For pulse-chase experiments, cells were treated with 5 μM MG132 simultaneous to the starvation, pulse, and chase period. Exogenous protein expression using the Flp-In T-REx-293 cell line was induced by doxycycline. In general, cells were incubated with a medium containing 1 μg/ml doxycycline (dissolved in water) for 16 h. For Flp-In T-REx-293 cells expressing N-terminally fused MTS-MIA40/CHCHD4 variants, 0.01 μg/ml doxycycline was used, while non-MTS-MIA40/CHCHD4 variants were induced with 0.1 μg/ml doxycycline. Doxycycline was applied for 1 h and then washed out, if not stated otherwise in the description of the individual experiment. Stable cell lines, created with the Piggy Bac Transposon system were induced with 30 μg/ml cumate (in ethanol), added to the medium, for 16 h

 © 2022 The Authors

or up to 3 days, if not stated otherwise in the description of the individual experiment. For siRNA-mediated gene silencing, cells were transfected with siRNA (Qiagen) (Appendix Table S1) using the transfection reagent Interferin (Polyplus) according to the manufacturer's protocol. The knockdown was performed for 48 (ALR depletion), 72, or 96 h (MIA40/CHCHD4 or AIFM1 depletion). The protein translation inhibitor emetine was applied to the cells for the respective time at a concentration of 100 µg/ml and added to the medium.

#### Analytical size-exclusion chromatography

Analytical size-exclusion chromatography was performed under native conditions to examine protein complexes between intact proteins. Cells were washed with 1x PBS and mechanically detached by scraping. Cells were sedimented at 500 *g* for 5 min. Pellets were resolved in 660 µl native lysis buffer (100 mM sodium phosphate pH 8.0, 100 mM sodium chloride, 1% (v/v) Triton X-100), supplemented with 0.2 mM PMSF. Mitochondria isolated from different mouse tissues (C57BL/6 NTac background) were lysed in the same native lysis buffer. Mitochondria were isolated as described in section "In organello import assay." Cells and mitochondria were lysed for 1 h on ice, and the lysate was cleared by centrifugation. Lysate was loaded on a HiLoad™ 16/600 Superdex 200 preparation grade gel filtration column and installed in a liquid chromatography system (Aekta Purifier) from GE Healthcare. A protein size standard was used as a reference, covering a range from 29 kDa to 700 kDa (#MWGF1000-1KT, Sigma-Aldrich).

#### Steady-state protein levels

Cells were washed with ice-cold PBS and lysed either by addition of Laemmli buffer (2% SDS, 60 mM Tris–HCl pH 6.8, 10% glycerol, 0.0025% bromophenol blue) or RIPA buffer (50 mM Tris–pH 8, 150 mM NaCl, 1% Triton X-100, 0.5% sodium deoxycholate, 0.1% SDS, 1x protease inhibitor cocktail). Laemmli lysis samples were boiled for 5 min at 96°C and analyzed via SDS–PAGE and immunoblotting. RIPA lysis samples were incubated for 1 h on ice and then centrifuged for 1 h at 20,000 *g* at 4°C. The protein concentration of the cleared lysate was determined via Roti-Quant universal kit (Carl Roth). Samples were supplemented with Laemmli buffer, containing in addition 50 mM Dithiothreitol. Samples were boiled for 5 min at 96°C and analyzed via SDS–PAGE and immunoblotting.

#### Immunoprecipitation

Immunoprecipitations were carried out either under native or denaturing lysis conditions. For both, cells were washed with 1x PBS, supplemented with 20 mM NEM (N-Ethylmaleimide). Cells were mechanically detached by scraping, after an incubation time of 10 min, on ice in 1x PBS + NEM. Cells were sedimented with 800 *g* for 5 min at 4°C and gently lysed in ice-cold native IP lysis buffer (100 mM sodium phosphate pH 8.0, 100 mM sodium chloride, 1% (v/v) Triton X-100, 0.2 mM PMSF) for 1 h on ice. Lysate was cleared by centrifugation 22,000 *g* 1 h at 4°C. Supernatant was transferred to a prewashed agarose matrix and incubated for 16 h at 4°C on a tumbling shaker.

For immunoprecipitation under denaturing conditions, cells were lysed in ice-cold denaturing IP lysis buffer (100 mM Tris–HCl, pH 8.1, 150 mM sodium chloride, 1 mM EDTA), supplemented with 1.6% (w/v) SDS. Lysate was sonicated or supplemented with Benzonase, respectively, and heated up to 96°C until DNA was degraded. Afterwards, triple the volume of denaturing IP buffer, containing 2.5% (v/v) Triton X-100 was added and samples were incubated for 1 h on ice. After a 1-h centrifugation step with 22,000 *g* at 4°C, the supernatant was transferred to a prewashed agarose matrix and incubated for 16 h at 4°C on a tumbling shaker. Afterwards, beads were triply washed with the respective IP lysis buffer, containing Triton X-100 and once finally washed with IP lysis buffer without Triton X-100. Precipitated proteins were eluted from the agarose matrix by addition of Laemmli buffer and heating up to 96°C for 3 min.

#### Assay to address inverse redox states of protein thiols

The steady-state redox state assay was performed as previously described (Erdogan *et al*, 2018). To trap the redox state *in situ*, the cells were incubated in PBS containing 20 mM NEM (N-ethylmaleimide, 0.125 kDa) for 10 min at 4°C, blocking reduced cysteines. Cells were triply washed with ice-cold 1x PBS. Subsequently, cells were lysed in Laemmli buffer and oxidized cysteines were reduced by the addition of 10 mM TCEP (Tris(2-carboxyethyl) phosphine) and incubated at either 4°C or 96°C for 15 and 10 min, respectively. Following, the newly reduced cysteines were modified with the alkylating agent $mmPEG_{12}$ (0.711 kDa). For maximal shift controls, the proteins were completely reduced without NEM treatment before modification, while the minimum shift samples were incubated with NEM only. Alkylation with $mmPEG_{12}$ was carried out for 1 h at room temperature. Subsequently, samples were separated by Tricine–PAGE and analyzed by western blot, followed by immunoblotting.

#### Oxidation kinetic assay

*Oxidation kinetic assays* to assess the oxidation of newly synthesized proteins over time in intact cells were performed as described previously (Fischer *et al*, 2013). Newly synthesized proteins were pulse labeled with EasyTag EXPRESS $^{35}S$ Protein Labeling Mix (Perkin Elmer) at a concentration of 200 µCi/ml and added to the medium. The pulse labeling was stopped by the addition of a chase medium containing 20 mM methionine and incubation for indicated times. The chase was stopped by the addition of Laemmli buffer, supplemented with 20 mM $mmPEG_{24}$ and $mmPEG_{12}$, respectively, except for the minimal and maximal shift approaches. The maximal shift approach was supplemented with 20 mM TCEP, heated up to 96°C for 10 min, and subsequently complemented with 20 mM $mmPEG_{24}$ and $mmPEG_{12}$, respectively. After modification with $mmPEG_{24}$, immunoprecipitation under denaturing conditions was performed, as described before.

#### SILAC-based mass spectrometry of AIFM1 knockout mitochondria

Dataset EV1 contains these data. Cells were grown as previously described (Stroud *et al*, 2016). Briefly, control and AIFM1 knockout cells were cultured in DMEM lacking L-arginine and L-lysine (Assay Matrix) supplemented with 10% (v/v) dialyzed FBS (GE

© 2022 The Authors

Healthcare), penicillin/streptomycin (Sigma-Aldrich), glutamax (Life Technologies), sodium pyruvate (Life Technologies) and 50 μg/ml uridine (Sigma-Aldrich) and 600 mg/l L-proline (Sigma-Aldrich). Heavy ($^{13}C_6{}^{15}N_4$-Arginine; $^{13}C_6{}^{15}N_2$-Lysine; Cambridge Isotope Labs) or light amino acids (Sigma-Aldrich) were added at 42 and 146 mg/l, respectively. Cells were cultured under these conditions for 1 month prior to analysis. Cells were harvested and SILAC label pairs combined based on protein concentration. Cell pellets were resuspended in 0.025% (w/v) digitonin (Merck), 20 mM HEPES pH 7.0 (Sigma-Aldrich), 250 mM sucrose (Sigma-Aldrich), 100 mM KCl (Sigma-Aldrich), 1 mM EDTA (Sigma-Aldrich) and gently lysed through repeated pipetting through a 1,000 μl tip. Lysate was incubated for 20 min on ice, followed by centrifugation at 800 *g* for 5 min at 4°C. The supernatant was subsequently centrifuged at 10,000 *g* for 10 min at 4°C to collect crude mitochondria. Crude mitochondria were solubilized in 1% (w/v) sodium deoxycholate (Sigma-Aldrich), 100 mM Tris–pH 8.1 (Sigma-Aldrich), and 40 mM chloroacetamide, and samples were boiled for 15 min with shaking. Cooled lysates were incubated with trypsin (Promega) per the manufacturer's instructions for 5 h at 37°C. Peptides were acidified with a 1:1 volume of 1% (v/v) trifluoracetic acid (TFA; Sigma-Aldrich) in ethyl acetate (Sigma-Aldrich) and the organic phase containing lipids and detergent removed by aspiration. The aqueous phase was loaded onto self-made 3x 14G 3M™Empore™ SDB-RPS stage tips as described (Kulak *et al*, 2014). The tips were washed with the above TFA/ethyl acetate solution followed by 0.2% (v/v) TFA and elution in 80% acetonitrile (v/v) (ACN; Sigma-Aldrich), 1% $NH_4OH$ (v/v) (Sigma-Aldrich). Peptides were acidified with TFA prior to drying in a vacuum concentrator.

Peptides were reconstituted in 2% (v/v) ACN and 0.1% (v/v) TFA, and transferred to autosampler vials for analysis online by nano-HPLC/electrospray ionization-MS/MS on a Thermo Fisher Scientific Orbitrap Q-Exactive Plus connected to an Ultimate 3000 HPLC (Thermo Fisher Scientific). Peptides were first loaded onto a trap column (Acclaim C18 PepMap nano Trap × 2 cm, 100 μm I.D, 5 μm particle size, and 300 Å pore size; Thermo Fisher Scientific) at 15 μl/min for 3 min before switching the precolumn in line with the analytical column (Acclaim RSLC C18 PepMap Acclaim RSLC nanocolumn 75 μm × 50 cm, PepMap100 C18, 3 μm particle size 100 Å pore size; Thermo Fisher Scientific). The separation of peptides was performed at 250 nl/min using a nonlinear ACN gradient of buffer A (0.1% formic acid [FA], 2% ACN) and buffer B (0.1% FA, 80% ACN), starting at 2.5% buffer B to 35.4% followed by ramp to 99% over 240 min (runs had a total acquisition time of 280 min to accommodate void and equilibration volumes). Data were collected in positive mode using Data Dependent Acquisition using m/z 375-1575 as MS scan range, HCD for MS/MS of the 12 most intense ions with $z \geq 2$. Other instrument parameters were MS1 scan at 70,000 resolution (at 200 m/z), MS maximum injection time 54 ms, AGC target 3e6, normalized collision energy was at 27% energy, isolation window of 1.8 Da, MS/MS resolution 17,500, MS/MS AGC target of 2E5, MS/MS maximum injection time of 54 ms, and minimum intensity was set at 2e3 and dynamic exclusion was set to 15 s.

Raw files were analyzed using the MaxQuant platform (Tyanova *et al*, 2016a) version 1.6.0.16 searching against a UniProt human database containing reviewed, canonical entries (September 2017) and a database containing common contaminants. The search was setup using default settings for a SILAC experiment with the following modifications: multiplicity set to 2 (Lys8, Arg10), deamidation (NQ) included as a variable modification and "Match between runs," was enabled. Data were processed using the Perseus platform (Tyanova *et al*, 2016b) version 1.5.5.3. Label switched samples (where AIFM1 knockout was labeled with light SILAC media) were inverted and "Normalized H/L ratios" were $Log_2$ transformed. Values listed as being "Only identified by site," "Reverse," or "Contaminants" were removed from the dataset. Mitochondrial annotations were imported by matching gene names and/or ENSG identifiers with the Mitocarta2.0 dataset (Calvo *et al*, 2016). A one-sample Student's two-sided *t*-test was performed across the replicates, and the negative logarithmic *P*-values were plotted against the differences between the mean ratios for each group. A significance threshold ($P < 0.05$) was used for all experiments.

#### Immunofluorescence

Immunofluorescence was used to analyze the subcellular localization of proteins of interest. Exogenous protein expression of Strep-tagged MIA40/CHCHD4 constructs in HEK293 Flp-In T-REx cells was induced by doxycycline for 16 h. Cells were grown on poly-L-lysine-coated coverslips. Doxycycline was washed out for 1 h, while cells were simultaneously treated with MitoTracker™ Deep Red, according to the manufacturer's specifications. Cells were fixed with 4% formaldehyde for 15 min. Then, cell membranes were permeabilized with blocking buffer (20 mM HEPES pH 7.4, 3% BSA, 0.3% Triton X-100) for 1 h. Cells were incubated with the primary antibody in blocking buffer for 16 h at 4°C and the secondary antibody (respective AlexaFluor 488 antibody) for 2 h at room temperature. Then, cells were incubated with 1 μg/ml DAPI for 15 min at room temperature. Coverslips were mounted onto microscope slides using mowiol, supplemented with DABCO. Cells were analyzed by confocal fluorescence microscopy.

#### BN–PAGE analysis

BN–PAGE analysis was performed as described in (Szczepanowska *et al*, 2020). In short, mitochondria were isolated from cultured cells by resuspending them in 20 mM HEPES pH 7.6, 220 mM mannitol, 70 mM sucrose, 1 mM EDTA, 0.2% fatty acid-free BSA, and homogenizing them with a rotating Teflon potter (40 strokes, 1,200 rpm) followed by differential centrifugation at 850 and 8,500 *g*, 10 min, 4°C. Mitochondrial protein concentrations were determined with Bradford reagent (Sigma). Equal amounts of mitochondria (15–25 μg) were lysed for 15 min on ice in dodecylmaltoside (DDM; 5 g/g of protein) and cleared from insoluble material for 20 min at 20,000 *g*, 4°C. Lysates were combined with Coomassie G-250 (0.25% final). Mitochondrial complexes were resolved with BN–PAGE using the 4–16% Native-PAGE Novex Bis-Tris Mini Gels (Invitrogen) in a Bis-Tris/Tricine buffering system with cathode buffer initially supplemented with 0.02% G-250 followed by the 0.002% G-250. Separated mitochondrial complexes were analyzed by immunoblotting with the indicated antibodies.

#### Complexome profiling

Complexomics from crude mitochondria was performed to analyze complexes of the respiratory chain (Guerrero-Castillo *et al*, 2017).

 © 2022 The Authors

Exogenous protein expression was started 4 days before mitochondria were isolated. For isolation of crude mitochondria, cells were detached by trypsin treatment. Cells were gently lysed on ice for 10 min in 1x PBS, supplemented with an EDTA-containing protease inhibitor cocktail, 500 units of Benzonase, and digitonin (150 μg per $1 \times 10^6$ cells). Mitochondria were pelleted at 8,500 *g* for 10 min. Mitochondrial protein concentrations were determined with Bradford reagent (Sigma). Crude mitochondria were washed in CCMI buffer (250 mM sucrose, 1 mM EDTA, 20 mM Tris–HCl pH 7.4) and stored at −80°C until use. For Blue Native–PAGE, crude mitochondria aliquots were thawed on ice, and 200 μg protein from each sample was resuspended in CCMI buffer plus proteases inhibitors cocktail and centrifuged at 22,000 *g*. Pellets were solubilized with 6 g digitonin per g protein in 40 μl ice-cold solubilization buffer (50 mM NaCl, 50 mM imidazole-HCl, 2 mM 6-aminohexanoic acid, 1 mM EDTA, pH 7.0) and centrifuged at 22,000 *g* for 20 min, 4°C. Supernatants were supplemented with Coomassie-blue G-250 (Serva G) and loaded on polyacrylamide gradient gels (4–16%). Electrophoretic run and Coomassie-blue staining were carried out as previously described (Wittig *et al*, 2006).

Proteins were identified by mass spectrometry (MS) after in-gel tryptic digestion essentially as performed in Heide *et al* (2012) with slight modifications. Briefly, each gel lane was cut into 60 even slices (~0.2 cm). Gel slices were diced in smaller fragments and transferred into 96-well filter plates (Millipore®, MABVN1250) adapted manually to 96-well plates (MaxiSorp™ Nunc) as waste collectors. Gel pieces were incubated with 50% methanol, 50 mM ammonium hydrogen carbonate (AHC) under gentle shaking and refreshed up until the blue dye was removed completely. Removal of the excess solution was done by centrifugation (1,000 *g*, 20 s). In order to reduce and block the cysteine thiol groups, the gel pieces were incubated with 1 mM dithiothreitol (DTT) in 50 mM AHC for 1 h. After removal of the excess solution by centrifugation, 30 mM chloroacetamide in 50 mM AHC was added to each well and removed after 45 min. A 15 min incubation step with 50% methanol and 50 mM AHC was done to dehydrate the gel pieces. After excess solution removal, the gel pieces were dried at room temperature for 30 min. Then, 20 μl of 5 ng·μl$^{-1}$ Trypsin (sequencing grade, Promega®) in 50 mM AHC plus 1 mM $CaCl_2$ were added to each well and incubated for 30 min at 4°C. A 50 μl of 50 mM AHC were further added to cover the gel pieces followed by overnight protein digestion at 37°C. The peptide-containing supernatants were collected by centrifugation (1,000 *g*, 1 min) into a clean 96-well PCR plate (Axygen®). In addition, the gel pieces were incubated once with 50 μl of 30% acetonitrile (ACN), 3% formic acid (FA) for 20 min and centrifuged (1,000 *g*, 1 min) to maximize peptide recovery. The combined eluates were dried in a SpeedVac Concentrator Plus (Eppendorf) and the peptides were finally resuspended in 20 μl of 5% ACN, 0.5% FA, and kept frozen at −20°C until use. Tryptic peptides were separated by reverse-phase liquid chromatography and analyzed by tandem MS in a Q-Exactive Orbitrap Mass Spectrometer equipped with an Easy nLC1000 nano-flow ultra-HPLC system (Thermo Fisher Scientific). In short, peptides were separated using 100 μm ID × 15 cm length PicoTip™ EMITTER columns (New Objective) filled with ReproSil-Pur C18-AQ reverse-phase beads (3 μm, 120 Å) (Dr. Maisch GmbH, Germany) using linear gradients of 5–35% ACN, 0.1% FA (30 min) at a flow rate of 300 nl min$^{-1}$, followed by 35–80% ACN, 0.1% FA (5 min) at 600 nl min$^{-1}$ and a final column wash with 80% ACN (5 min) at 600 nl min$^{-1}$. All settings for the mass spectrometer operation were the same as those detailed in Guerrero-Castillo *et al*, 2017.

MS raw data files were analyzed using MaxQuant (v1.5.0.25) using the settings previously described in (Huynen *et al*, 2016). For identification, spectra were matched against a database including all the human protein sequences retrieved from Uniprot (December 2019). Individual protein abundance was determined by label-free quantification using the obtained intensity-based absolute quantification (iBAQ) values. The latter was corrected for protein loading and MS sensitivity variations using the sum of iBAQ values of the MitoCarta 2.0 TRUE proteins identified in each sample. For each protein, gel migration profiles were generated and normalized to the maximum abundance through all fractions analyzed. The migration patterns of the identified proteins were hierarchically clustered by an average linkage algorithm with centered Pearson correlation distance measures. The resultant complexome profiles consisting of a list of proteins arranged according to the similarity of their migration patterns in the BN–PAGE were visualized as heat maps representing the normalized abundance in each gel slice by a three-color gradient (black/yellow/red) and processed in Microsoft Excel for further analysis. The internal mass calibration for either membrane or soluble proteins was done using the apparent molecular masses of known complexes. Raw data were uploaded to the CEDAR database (https://www3.cmbi.umcn.nl/cedar/browse/) with the accession code CRX34.

#### Activity assays of respiratory chain complexes

For this procedure, crude mitochondria were generated as described before for complexomics, with one exception, cells were gently lysed in 1x PBS supplemented with 0.5 mM EDTA, 500 units Benzonase, and digitonin (150 μg per $1 \times 10^6$ cells). On the day of the measurements, crude mitochondria aliquots from each sample (4–7 biological replicates) were thawed on ice and the protein concentration was determined using the DC method (Bio-Rad). Samples were diluted in 2 ml CCMI buffer plus 1 mg·ml$^{-1}$ fatty acid-free BSA and homogenized with 15 gentle strokes in ice-cold Potter-Elvehjem tubes. Mitochondria were pelleted by centrifugation at 22,000 *g* for 20 min. In order to disrupt the mitochondrial membranes and expose all matrix-sided catalytic sites, pellets were resuspended in 20 mM Tris–HCl, pH 7.4 to a final concentration of 0.5 mg prot·ml$^{-1}$ and subjected to three freeze–thaw cycles using liquid nitrogen.

Enzyme activities of the respiratory chain complexes were determined spectrophotometrically based on the protocols described in (Barrientos *et al*, 2009; Spinazzi *et al*, 2012) with modifications. Here, the assays were performed using 96-wells plates (MaxiSorp™ Nunc) in a SPECTRAmax ABC PLUS plate reader (Molecular Devices) at 32°C. In all cases, the final concentration of mitochondrial membranes and reaction volume per well were 50–100 μg protein·ml$^{-1}$ and 200 μl, respectively.

*Complex I* activity was determined as the rotenone-sensitive NADH oxidase activity following the oxidation of NADH at 340 nm ($\varepsilon_{340nm}$ = 6.22 mM$^{-1}$·cm$^{-1}$). Mitochondrial membranes were added to a reaction mixture containing 25 mM potassium phosphate, pH 7.5, 1 mg·ml$^{-1}$ fatty acid-free BSA, and 20 μM horse-heart cytochrome *c*. 100 μl of this mixture were distributed into the

© 2022 The Authors

wells and the reaction was started by the addition of 100 µl of 240 µM NADH in 25 mM potassium phosphate, pH 7.5 (final conc. 120 µM). NADH oxidation was recorded for 2 min. Then, 25 µM rotenone was added to inhibit complex I, and the residual absorbance changes were recorded for 3 min.

*Complex II* (succinate:ubiquinone oxidoreductase) activity was measured by following the reduction in 2,6-dichlorophenolindophenol (DCPIP) at 600 nm ($\varepsilon_{600nm}$ = 19.1 $mM^{-1}\cdot cm^{-1}$). Mitochondrial membranes were preincubated in 195 µl of reaction buffer consisting of 20 mM Tris–HCl, pH 7.2, 1 $mg\cdot ml^{-1}$ fatty acid-free BSA, 10 µM rotenone, 2 µM myxothiazol, 500 µM NaCN, 80 µM DCPIP and 10 mM succinate for 10 min at room temperature. Afterwards, the reaction was initiated with 5 µl of 2.8 mM decylubiquinone in DMSO (final conc. 70 µM) and recorded for 3–5 min. 10 mM malonate was added to inhibit complex II and the residual absorbance changes were recorded for 3 min.

*Complex III* (decylubiquinol:cytochrome *c* oxidoreductase) activity was measured by monitoring the reduction in horse-heart cytochrome *c* at 550 nm ($\varepsilon_{550nm}$ = 18.5 $mM^{-1}\cdot cm^{-1}$). 100 µl of a reaction mixture consisting of 25 mM potassium phosphate, pH 7.5, 10 µM rotenone, 500 µM NaCN, 0.1 mM EDTA, 100 µM decylubiquinol, and the mitochondrial membranes were distributed into the wells. The reaction assay was started by the addition of 100 µl of 150 µM oxidized horse-heart cytochrome *c* in 25 mM potassium phosphate (pH 7.5) (final conc. 75 µM). The initial activities were monitored for 2 min; afterwards, complex III was inhibited with 5 µM myxothiazol, and the residual absorbance changes were recorded for 3 min.

*Complex IV* (cytochrome *c* oxidase) activity was determined by following the oxidation of reduced horse-heart cytochrome *c* at 550 nm. Mitochondrial membranes were dissolved in 25 mM potassium phosphate (pH 7) plus 2 µM myxothiazol. 100 µl of this mixture were distributed into the wells and the reaction was started with 100 µl of 150 µM reduced horse-heart cytochrome *c* (final conc. 75 µM). Cytochrome c oxidation was monitored for 3–5 min. 1 mM NaCN was added to inhibit complex IV and the residual absorbance changes were recorded for 3 min.

Specific inhibitor-sensitive activities of all respiratory complexes in each sample were calculated by subtracting the residual inhibitor-insensitive activities from the initial activities and measured in at least 3 technical replicates. To avoid activity variations due to differences in the mitochondrial protein content among the samples, all the specific activities were normalized against their complex II specific activities.

### In organello import assay

This experiment has been performed as previously described (Murschall *et al*, 2020, 2021). For the isolation of crude mitochondria, cells were washed in PBS and resuspended in homogenization buffer (220 mM mannitol, 70 mM sucrose, 5 mM HEPES/KOH pH 7.4, 1 mM EGTA) prior to homogenization with a rotating Teflon potter (*Potter S*, *Braun*). The homogenate was cleared of debris and nuclei by centrifugation at 600 *g* for 5 min at 4°C. The supernatant was centrifuged at 8,000 *g* for 10 min at 4°C to obtain mitochondrial fractions. Mitochondria were washed in homogenization buffer and 20 µg was taken per import reaction. Radiolabeled precursor proteins were synthesized for 1 h at 30°C using the SP6 promoter TNT Quick Coupled Transcription/Translation System (*Promega*) containing 20 µCi [$^{35}$S]-methionine. Protein import was initiated by incubating precursor protein with crude mitochondria at 30°C in the presence or absence of CCCP (1 mM). Import was stopped after 10, 30, or 60 min by placing mitochondria on ice. All samples were treated with proteinase K (20 µg $ml^{-1}$) for 20 min to degrade nonimported precursor protein. Mitochondria were then washed in homogenization buffer containing PMSF (1 mM) and resuspended in Laemmli buffer for analysis by SDS–PAGE and autoradiography.

### Peptide synthesis

The peptides GSEGKDRIIFVTKEDHETPSSAEL-$NH_2$ ($MW_{calc}$ = 2644.86 Da; $MW_{exp}$ = 2645.26 Da), and CF-GSEGKDRIIFVTKE DHETPSSAEL-$NH_2$ ($MW_{calc}$ = 3003.18 Da; $MW_{exp}$ = 3004.08 Da) were synthesized by standard fluorenylmethoxycarbonyl (Fmoc) solid-phase peptide synthesis on Rink amide resin (0.48 mmol/g, 15 µmol scale) using an automated peptide synthesizer (Syro I, MultiSynTech). Amino acid couplings were done using eight equivalents each of OxymaPure (2-cyano-2(hydroxyamino)acetate), DIC (dicyclohexylcarbodiimide), and the respective fully protected amino acid in DMF (dimethylformamide). Fmoc removal was performed by incubating the resin first with a 40%, then with a 20% solution of piperidine in DMF.

The fluorophore 5,6-carboxyfluorescein (CF) was coupled manually by incubating the resin with two equivalents CF and two equivalents HATU (*O*-(7-azabenzotriazol-1-yl)-N,N,N′,N′-tetramethyluronium-hexafluorphosphate) and two equivalents of DIPEA (N,N-diisopropylethylamine).

Peptides were cleaved from the resin using a mixture of 95/2.5/2.5 (v/v/v) concentrated trifluoroacetic acid (TFA)/water/TIS (triisopropylsilane). The resulting peptides were purified by reverse-phase HPLC using a linear gradient of 15–50% B in A (A: water/0.1% TFA; B: acetonitrile (ACN)/0.08% TFA) for the unlabeled peptide and 20–60% B in A for the CF-labeled peptide. Purity was > 95% for all peptides.

### *In vitro* reconstitution of the AIFM1-MIA40/CHCHD4 interaction and ITC

#### *Protein purification*

Recombinant MIA40/CHCHD4$^{C4S,C53S,C55S}$ or Δ1-40 MIA40/CHCHD4$^{C53S,C55S}$ was expressed from a pET24a(+) expression vector in *Escherichia coli* Rosetta 2 cells. Recombinant AIFM1(103–613) was expressed from a pET24a(+) or pGEX-4t-1 expression vector in *Escherichia coli* Rosetta 2 cells. Bacterial growth was conducted in LB media (for AIFM1 supplemented with riboflavin and FAD) prior to induction of protein expression with 1 mM IPTG. Cultures were incubated at 37°C and 110 rpm shaking for 16–20 h. Affinity purification of GST-tagged AIFM1(103–613) was performed at 4°C for 16 h using glutathione Sepharose (4 Fast Flow, GE) in binding buffer (20 mM Tris–HCl pH 7.4, 200 mM NaCl). AIFM1 (103–613) was either released from GSH beads by thrombin-mediated tag cleavage in PBS pH 7.4 or kept coupled to beads for subsequent CHCHD4/MIA40 peptide binding assays.

For 6xHis-tagged AIFM1(103–613) and the two 6xHis-tagged MIA40/CHCHD4 constructs, Immobilized Metal Affinity Chromatography using Ni Sepharose (6 Fast Flow, GE) was conducted. The

 © 2022 The Authors

bacterial lysate was bound to beads in binding buffer supplemented with 10 mM imidazole at 4°C for 90 min. Beads were washed once with binding buffer supplemented with 20 mM imidazole prior to elution with 250 mM imidazole. Recombinant AIFM1(103–613) was dialyzed (MW cut-off 3.5 kDa) against PBS pH 7.4 for storage and subsequent ITC experiments.

#### *Peptide assay*

If not stated otherwise, empty glutathione sepharose beads or beads loaded with GST-AIFM1 were incubated with 10 μM carboxyfluorescein (CF)-labeled fluorescent CHCHD4/MIA40 peptide in binding buffer supplemented with 0.1 mM NADH for 30 min at room temperature. Beads were centrifuged at 2,000 *g* for 30 s and supernatant was obtained for analysis of *unbound* fractions. After three washing steps with binding buffer + NADH, both supernatant and beads were used for fluorescence analysis as *wash* and *bound* fraction, respectively. Fluorescence was measured at an excitation wavelength of 483 ± 7 nm and an emission wavelength of 530 ± 15 nm.

#### *Establishment of the AIFM1-MIA40/CHCHD4 complex with purified proteins*

The AIFM1 MIA40/CHCHD4 complex was reconstituted by combining the recombinant proteins in a 1:2.7 (AIFM1:MIA40/CHCHD4) molar ratio and dialysis against 60 mM NaCl, 60 mM $NaP_i$ pH = 7.4 containing 0.1 mM NADH. The complex was separated from monomeric MIA40/CHCHD4 on a 16/600 Superdex 200 PG column by injecting a 1-ml sample with a total protein content of 250 nmol. The buffer contained 0.1 mM NADH, 60 mM NaCl, 60 mM $NaP_i$ pH = 7.4. All steps were performed at 4°C.

#### *ITC*

Isothermal titration calorimetry was performed at 25°C on a MicroCal Auto-ITC200 (Malvern, United Kingdom). For analysis of the interaction between AIFM1 and MIA40/CHCHD4 peptide, 6xHis-tagged AIFM1(103–613) was dialyzed against PBS pH 7.4 supplemented with 0.1 mM NADH at 4°C for 17 h. Lyophilized unlabeled CHCHD4/MIA40 peptide was dissolved in dialysis buffer to a final concentration of 200 μM. The concentration of 6x-His-AIFM1(103–613) in the sample cell was 16.9 μM. Measurements were carried out by 2 μl injections of the CHCHD4/MIA40 peptide into the cell with an injection duration of 4 s. Ultimately, 19 injections were performed during the titration. For data correction, CHCHD4/MIA40 For ITC with recombinant proteins, purified proteins were dialyzed against 60 mM NaCl, 60 mM $NaPO_i$ pH = 7.4 containing 0.1 mM NADH. AIFM1 was diluted to 20 μM and MIA40/CHCHD4 and Δ1-40 MIA40/CHCHD4 to 200 μM, respectively. Artificial signals were excluded by the additional measurement of each protein against the used buffer.

#### Quantification and statistical analysis

Intensities of autoradiography and immunoblot signals were quantified using ImageQuantTL (*GE*) and Image Lab (Bio-Rad Laboratories), respectively. For SILAC MS data interpretation, Perseus software was used (Tyanova *et al*, 2016b). Error bars in figures represent standard deviation. The number of experiments is reported in the figure legend.

## Data availability

The datasets of the complexome profiling experiments in the current study are available in the CEDAR database (https://www3.cmbi.umcn.nl/cedar/browse/) with the accession code CRX34 (https://www3.cmbi.umcn.nl/cedar/browse/experiments/CRX34). Further datasets generated during and/or analyzed during the current study are available from the corresponding author upon reasonable request.

**Expanded View** for this article is available online.


### Acknowledgements

The Deutsche Forschungsgemeinschaft (DFG, German Research Foundation) funds research in the Laboratory of JR through the grants RI2150/5-1, RI2150/2-2, RTG2550/1, and CRC1218—Project number 269925409. Research in the lab of UB is funded by CRC1218—Project number 269925409 and grants from the Netherlands Organization for Health Research and Development (TOP 91217009) and the Netherlands Organization for Scientific Research (TOP 714.017.00 4). Research in the lab of AT is funded by the Deutsche Forschungsgemeinschaft (DFG, German Research Foundation) including CRC1218—Project number 269925409. We thank the Monash Biomedical Proteomics Facility and Monash Flowcore for the provision of instrumentation, training, and technical support. We acknowledge funding from the National Health and Medical Research Council (NHMRC Project Grants 1164459 to MTR; 1125390, 1140906 to MTR and DAS; NHMRC Fellowship 1140851 to DAS). We thank the CECAD Proteome and Imaging Facilities for the provision of instrumentation, training, and technical support. Open Access funding enabled and organized by Projekt DEAL.


### Author contributions

**Silja, Lucia Salscheider:** Formal analysis; investigation; methodology. **Sarah Gerlich:** Investigation; methodology; writing – review and editing. **Alfredo Cabrera-Orefice:** Data curation; investigation; methodology; writing – review and editing. **Esra Peker:** Investigation; methodology. **Robin Alexander Rothemann:** Investigation; methodology. **Lena Murschall:** Investigation; methodology. **Yannik Finger:** Investigation; methodology. **Karolina Szczepanowska:** Investigation; methodology. **Zeinab, Alsadat Ahmadi:** Investigation; methodology. **Sergio Guerrero-Castillo:** Investigation; methodology. **Alican Erdogan:** Investigation; methodology. **Mark Becker:** Investigation; methodology. **Muna Ali:** Investigation; methodology. **Markus Habich:** Investigation; methodology. **Carmelina Petrungaro:** Investigation; methodology. **Nele Burdina:** Investigation; methodology. **Guenter Schwarz:** Data curation; formal analysis; writing – review and editing. **Merlin Klussmann:** Investigation; methodology. **Ines Neundorf:** Data curation; formal analysis; writing – review and editing. **David A Stroud:** Data curation; formal analysis; investigation; methodology; writing – review and editing. **Michael T Ryan:** Formal analysis; investigation; writing – review and editing. **Aleksandra Trifunovic:** Formal analysis; investigation; writing – review and editing. **Ulrich Brandt:** Conceptualization; formal analysis; supervision; investigation; visualization; writing – original draft; writing – review and editing. **Jan Riemer:** Conceptualization; formal analysis; supervision; funding acquisition; validation; visualization; writing – original draft; project administration; writing – review and editing.

In addition to the CRediT author contributions listed above, the contributions in detail are:

J.R., U.B., and S.L.S. designed the study and planned experiments. All authors performed the experiments and/or analyzed the data. I.N. and M.K. synthesized the peptides. D.S. performed proteomic analysis. J.R. and U.B. wrote the manuscript with critical input from all authors.

© 2022 The Authors

### Disclosure and competing interests statement

The authors declare that they have no conflicts of interest.

## References


Agip AA, Blaza JN, Bridges HR, Viscomi C, Rawson S, Muench SP, Hirst J (2018) Cryo-EM structures of complex I from mouse heart mitochondria in two biochemically defined states. *Nat Struct Mol Biol* 25: 548 – 556

Banci L, Bertini I, Cefaro C, Ciofi-Baffoni S, Gallo A, Martinelli M, Sideris DP, Katrakili N, Tokatlidis K (2009) MIA40 is an oxidoreductase that catalyzes oxidative protein folding in mitochondria. *Nat Struct Mol Biol* 16: 198 – 206

Banci L, Bertini I, Cefaro C, Cenacchi L, Ciofi-Baffoni S, Felli IC, Gallo A, Gonnelli L, Luchinat E, Sideris D *et al* (2010) Molecular chaperone function of Mia40 triggers consecutive induced folding steps of the substrate in mitochondrial protein import. *Proc Natl Acad Sci U S A* 107: 20190 – 20195

Bano D, Prehn JHM (2018) Apoptosis-inducing factor (AIF) in physiology and disease: the tale of a repented natural born killer. *EBioMedicine* 30: 29 – 37

Barrientos A, Fontanesi F, Diaz F (2009) Evaluation of the mitochondrial respiratory chain and oxidative phosphorylation system using polarography and spectrophotometric enzyme assays. *Curr Protoc Hum Genet* Chapter: Unit19.3 https://doi.org/10.1002/0471142905.hg1903s63

Bihlmaier K, Mesecke N, Terziyska N, Bien M, Hell K, Herrmann JM (2007) The disulfide relay system of mitochondria is connected to the respiratory chain. *J Cell Biol* 179: 389 – 395

Calvo SE, Clauser KR, Mootha VK (2016) MitoCarta2.0: An updated inventory of mammalian mitochondrial proteins. *Nucleic Acids Res* 44: D1251 – D1257

Chacinska A, Guiard B, Muller JM, Schulze-Specking A, Gabriel K, Kutik S, Pfanner N (2008) Mitochondrial biogenesis, switching the sorting pathway of the intermembrane space receptor Mia40. *J Biol Chem* 283: 29723 – 29729

Elguindy MM, Nakamaru-Ogiso E (2015) Apoptosis-inducing factor (AIF) and its family member protein, AMID, are rotenone-sensitive NADH:Ubiquinone oxidoreductases (NDH-2). *J Biol Chem* 290: 20815 – 20826

Erdogan AJ, Ali M, Habich M, Salscheider SL, Schu L, Petrungaro C, Thomas LW, Ashcroft M, Leichert LI, Roma LP *et al* (2018) The mitochondrial oxidoreductase CHCHD4 is present in a semi-oxidized state *in vivo*. *Redox Biol* 17: 200 – 206

Fischer M, Horn S, Belkacemi A, Kojer K, Petrungaro C, Habich M, Ali M, Kuttner V, Bien M, Kauff F *et al* (2013) Protein import and oxidative folding in the mitochondrial intermembrane space of intact mammalian cells. *Mol Biol Cell* 24: 2160 – 2170

Friederich MW, Erdogan AJ, Coughlin CR 2nd, Elos MT, Jiang H, O'Rourke CP, Lovell MA, Wartchow E, Gowan K, Chatfield KC *et al* (2017) Mutations in the accessory subunit NDUFB10 result in isolated complex I deficiency and illustrate the critical role of intermembrane space import for complex I holoenzyme assembly. *Hum Mol Genet* 26: 702 – 716

Guerrero-Castillo S, Baertling F, Kownatzki D, Wessels HJ, Arnold S, Brandt U, Nijtmans L (2017) The assembly pathway of mitochondrial respiratory chain complex I. *Cell Metab* 25: 128 – 139

Habich M, Salscheider SL, Murschall LM, Hoehne MN, Fischer M, Schorn F, Petrungaro C, Ali M, Erdogan AJ, Abou-Eid S *et al* (2019) Vectorial import via a metastable disulfide-linked complex allows for a quality control step and import by the mitochondrial disulfide relay. *Cell Rep* 26: 759 – 774.e5

Hangen E, Feraud O, Lachkar S, Mou H, Doti N, Fimia GM, Lam NV, Zhu C, Godin I, Muller K *et al* (2015) Interaction between AIF and CHCHD4 regulates respiratory chain biogenesis. *Mol Cell* 58: 1001 – 1014

Heide H, Bleier L, Steger M, Ackermann J, Drose S, Schwamb B, Zornig M, Reichert AS, Koch I, Wittig I *et al* (2012) Complexome profiling identifies TMEM126B as a component of the mitochondrial complex I assembly complex. *Cell Metab* 16: 538 – 549

Hofmann S, Rothbauer U, Muhlenbein N, Baiker K, Hell K, Bauer MF (2005) Functional and mutational characterization of human MIA40 acting during import into the mitochondrial intermembrane space. *J Mol Biol* 353: 517 – 528

Huynen MA, Muhlmeister M, Gotthardt K, Guerrero-Castillo S, Brandt U (2016) Evolution and structural organization of the mitochondrial contact site (MICOS) complex and the mitochondrial intermembrane space bridging (MIB) complex. *Biochim Biophys Acta* 1863: 91 – 101

Joza N, Oudit GY, Brown D, Benit P, Kassiri Z, Vahsen N, Benoit L, Patel MM, Nowikovsky K, Vassault A *et al* (2005) Muscle-specific loss of apoptosis-inducing factor leads to mitochondrial dysfunction, skeletal muscle atrophy, and dilated cardiomyopathy. *Mol Cell Biol* 25: 10261 – 10272

Klein JA, Longo-Guess CM, Rossmann MP, Seburn KL, Hurd RE, Frankel WN, Bronson RT, Ackerman SL (2002) The harlequin mouse mutation downregulates apoptosis-inducing factor. *Nature* 419: 367 – 374

Kulak NA, Pichler G, Paron I, Nagaraj N, Mann M (2014) Minimal, encapsulated proteomic-sample processing applied to copy-number estimation in eukaryotic cells. *Nat Methods* 11: 319 – 324

McKenzie M, Ryan MT (2010) Assembly factors of human mitochondrial complex I and their defects in disease. *IUBMB Life* 62: 497 – 502

Mesecke N, Terziyska N, Kozany C, Baumann F, Neupert W, Hell K, Herrmann JM (2005) A disulfide relay system in the intermembrane space of mitochondria that mediates protein import. *Cell* 121: 1059 – 1069

Meyer K, Buettner S, Ghezzi D, Zeviani M, Bano D, Nicotera P (2015) Loss of apoptosis-inducing factor critically affects MIA40 function. *Cell Death Dis* 6: e1814

Mohanraj K, Wasilewski M, Beninca C, Cysewski D, Poznanski J, Sakowska P, Bugajska Z, Deckers M, Dennerlein S, Fernandez-Vizarra E *et al* (2019) Inhibition of proteasome rescues a pathogenic variant of respiratory chain assembly factor COA7. *EMBO Mol Med* 11: e9561

Montague TG, Cruz JM, Gagnon JA, Church GM, Valen E (2014) CHOPCHOP: A CRISPR/Cas9 and TALEN web tool for genome editing. *Nucleic Acids Res* 42: W401 – W407

Murari A, Rhooms SK, Goparaju NS, Villanueva M, Owusu-Ansah E (2020) An antibody toolbox to track complex I assembly defines AIF's mitochondrial function. *J Cell Biol* 219

Murschall LM, Gerhards A, MacVicar T, Peker E, Hasberg L, Wawra S, Langer T, Riemer J (2020) The C-terminal region of the oxidoreductase MIA40 stabilizes its cytosolic precursor during mitochondrial import. *BMC Biol* 18: 96

Murschall LM, Peker E, MacVicar T, Langer T, Riemer J (2021) Protein import assay into mitochondria isolated from human cells. *Bio Protoc* 11: e4057

Peleh V, Cordat E, Herrmann JM (2016) Mia40 is a trans-site receptor that drives protein import into the mitochondrial intermembrane space by hydrophobic substrate binding. *eLife* 5: e16177

Petrungaro C, Zimmermann KM, Kuttner V, Fischer M, Dengjel J, Bogeski I, Riemer J (2015) The Ca(2+)-dependent release of the Mia40-Induced MICU1-MICU2 dimer from MCU regulates mitochondrial Ca(2+) Uptake. *Cell Metab* 22: 721 – 733

Pospisilik JA, Knauf C, Joza N, Benit P, Orthofer M, Cani PD, Ebersberger I, Nakashima T, Sarao R, Neely G *et al* (2007) Targeted deletion of AIF decreases mitochondrial oxidative phosphorylation and protects from obesity and diabetes. *Cell* 131: 476 – 491


 © 2022 The Authors

Ran FA, Hsu PD, Wright J, Agarwala V, Scott DA, Zhang F (2013) Genome engineering using the CRISPR-Cas9 system. *Nat Protoc* 8: 2281 – 2308

Rissler M, Wiedemann N, Pfannschmidt S, Gabriel K, Guiard B, Pfanner N, Chacinska A (2005) The essential mitochondrial protein Erv1 cooperates with Mia40 in biogenesis of intermembrane space proteins. *J Mol Biol* 353: 485 – 492

Romero-Tamayo S, Laplaza R, Velazquez-Campoy A, Villanueva R, Medina M, Ferreira P (2021) W196 and the beta-hairpin motif modulate the redox switch of conformation and the biomolecular interaction network of the apoptosis-inducing factor. *Oxid Med Cell Longev* 2021: 6673661

Spinazzi M, Casarin A, Pertegato V, Salviati L, Angelini C (2012) Assessment of mitochondrial respiratory chain enzymatic activities on tissues and cultured cells. *Nat Protoc* 7: 1235 – 1246

Stroud DA, Surgenor EE, Formosa LE, Reljic B, Frazier AE, Dibley MG, Osellame LD, Stait T, Beilharz TH, Thorburn DR *et al* (2016) Accessory subunits are integral for assembly and function of human mitochondrial complex I. *Nature* 538: 123 – 126

Susin SA, Lorenzo HK, Zamzami N, Marzo I, Snow BE, Brothers GM, Mangion J, Jacotot E, Costantini P, Loeffler M *et al* (1999) Molecular characterization of mitochondrial apoptosis-inducing factor. *Nature* 397: 441 – 446

Szczepanowska K, Senft K, Heidler J, Herholz M, Kukat A, Hohne MN, Hofsetz E, Becker C, Kaspar S, Giese H *et al* (2020) A salvage pathway maintains highly functional respiratory complex I. *Nat Commun* 11: 1643

Szklarczyk R, Wanschers BF, Nabuurs SB, Nouws J, Nijtmans LG, Huynen MA (2011) NDUFB7 and NDUFA8 are located at the intermembrane surface of complex I. *FEBS Lett* 585: 737 – 743

Troulinaki K, Buttner S, Marsal Cots A, Maida S, Meyer K, Bertan F, Gioran A, Piazzesi A, Fornarelli A, Nicotera P *et al* (2018) WAH-1/AIF regulates mitochondrial oxidative phosphorylation in the nematode Caenorhabditis elegans. *Cell Death Discov* 4: 2

Tyanova S, Temu T, Cox J (2016a) The MaxQuant computational platform for mass spectrometry-based shotgun proteomics. *Nat Protoc* 11: 2301 – 2319

Tyanova S, Temu T, Sinitcyn P, Carlson A, Hein MY, Geiger T, Mann M, Cox J (2016b) The Perseus computational platform for comprehensive analysis of (prote)omics data. *Nat Methods* 13: 731 – 740

Ugalde C, Vogel R, Huijbens R, Van Den Heuvel B, Smeitink J, Nijtmans L (2004) Human mitochondrial complex I assembles through the combination of evolutionary conserved modules: a framework to interpret complex I deficiencies. *Hum Mol Genet* 13: 2461 – 2472

Vahsen N, Cande C, Briere JJ, Benit P, Joza N, Larochette N, Mastroberardino PG, Pequignot MO, Casares N, Lazar V *et al* (2004) AIF deficiency compromises oxidative phosphorylation. *EMBO J* 23: 4679 – 4689

Van Strien J, Guerrero-Castillo S, Chatzispyrou IA, Houtkooper RH, Brandt U, Huynen MA (2019) COmplexome profiling ALignment (COPAL) reveals remodeling of mitochondrial protein complexes in Barth syndrome. *Bioinformatics* 35: 3083 – 3091

Wang D, Eraslan B, Wieland T, Hallstrom B, Hopf T, Zolg DP, Zecha J, Asplund A, Li LH, Meng C *et al* (2019) A deep proteome and transcriptome abundance atlas of 29 healthy human tissues. *Mol Syst Biol* 15: e8503

Wischhof L, Gioran A, Sonntag-Bensch D, Piazzesi A, Stork M, Nicotera P, Bano D (2018) A disease-associated Aifm1 variant induces severe myopathy in knockin mice. *Mol Metab* 13: 10 – 23

Wittig I, Braun HP, Schagger H (2006) Blue native PAGE. *Nat Protoc* 1: 418 – 428

Zhu J, Vinothkumar KR, Hirst J (2016) Structure of mammalian respiratory complex I. *Nature* 536: 354 – 358

**License:** This is an open access article under the terms of the Creative Commons Attribution-NonCommercial-NoDerivs License, which permits use and distribution in any medium, provided the original work is properly cited, the use is non-commercial and no modifications or adaptations are made.